

# The Fate of Sediment After a Large Earthquake

Oliver Richard Francis<sup>1,1,1</sup>, Xuanmei Fan<sup>2,2,2</sup>, Tristram Charles Hales<sup>3,3,3</sup>, Daniel Edward James Hobley<sup>4,4,4</sup>, qiang xu<sup>2,2,2</sup>, and Huang Runqui<sup>2,2,2</sup>

<sup>1</sup>Helmholtz-Zentrum Potsdam - Deutsches Geoforschungszentrum

<sup>2</sup>Chengdu University of Technology

<sup>3</sup>Cardiff University

<sup>4</sup>University of Colorado Boulder

November 30, 2022

## Abstract

Large earthquakes cause rapid denudation of hillslopes by triggering thousands of coseismic landslides. The sediment produced by these landslides is initially mobilised out of the landscape as a cascade of unknown magnitude. This cascade dramatically enhances local erosion rates before rapidly returning to pre-earthquake levels. Identifying the individual processes of this cascade and estimating the volume of sediment they mobilise is crucial to determining the timescales over which earthquakes can influence hazards and sedimentary systems. Here we present a fully constrained sediment budget of the first decade after the 2008 Mw 7.9 Wenchuan earthquake. With this budget we identify the key erosion processes within the post seismic sediment cascade and constrain estimates of the volume of sediment removed from the landscape. With these estimates we find that over 90% of the coseismically generated sediment remaining on the hillslope 10 years after the earthquake. Despite the large volumes of sediment on the hillslope, we observe an order of magnitude decrease in the erosion rate of the epicentral area. Debris flows are the key erosional mechanism of the coseismically generated sediment as erosion rates are correlated with debris flow frequency. Erosion rates likely remain elevated for several decades however, the rapid stabilisation of the sediment following the earthquake suggests large volumes of coseismically generated sediment can remain in orogens for hundreds or thousands of years. In the most tectonically active regions, the long residence times of coseismically generated sediment could significantly reduce bedrock incision rates in channels altering long term erosion rates.

## **The Fate of Sediment After a Large Earthquake**

**Oliver Francis<sup>1,2,\*</sup>, Xuanmei Fan<sup>3</sup>, Tristram Hales<sup>1,2</sup>, Daniel Hobley<sup>2</sup>, Qiang Xu<sup>3</sup>, Runqiu Huang<sup>3</sup>.**

<sup>1</sup>Sustainable Places Research Institute, Cardiff University, Cardiff, United Kingdom

<sup>2</sup>School of Earth and Environmental Sciences, Cardiff University, Cardiff, United Kingdom

<sup>3</sup>State Key Laboratory for Geohazard Prevention and Geoenvironment Protection, Chengdu University of Technology, Chengdu, China

Corresponding author: Oliver Francis ([Oliver.Francis@gfz-potsdam.de](mailto:Oliver.Francis@gfz-potsdam.de))

\*Now at Section 4.7: Earth Surface Process Modelling, German Research Centre for Geosciences (GFZ), Potsdam, Germany

### **Key Points:**

- More than 88% (468 Mt) of sediment produced by the 2008  $M_w$ 7.9 Wenchuan earthquake remains on the hillslope 10 years after the event.
- Debris flows rather than fluvially driven erosion are the key process in transporting sediment from the hillslope into the main river.
- Evacuation of landslide deposits is highly stochastic indicating the need for long observation periods to estimate residence time.

## Abstract

Large earthquakes rapidly denude hillslopes by triggering thousands of coseismic landslides. The sediment produced by these landslides is initially quickly mobilised from the landscape by an interconnected cascade of processes. This cascade can dramatically but briefly enhance local erosion rates. Hillslope and channel processes, such as landsliding and debris flows, interact to influence the total mass, calibre, and rate of sediment transport through catchments. Calculating the sediment budget of an earthquake lends insight into the nature of these interactions. Using satellite imagery derived landslide inventories, channel surveys and a literature review combined with a Monte Carlo simulation approach we present a constrained sediment budget of the first decade after the 2008  $M_w$ 7.9 Wenchuan earthquake. With this sediment budget we demonstrate that debris flows are dominant process for delivering sediment into channels and that large volumes of sediment remain in the landscape. In our study area over 88% (469 Mega tonnes) of the coseismically generated sediment remains on the hillslopes in 2018. Of the 12% of the sediment that was mobilised, 69% ( $40.7 \pm 14$  Mt) was mobilised by debris flows. Despite the large proportion of sediment remaining on the hillslope, the frequency of debris flows declined significantly over our observation period. The reduction in debris-flow frequency is not correlated to reductions in the frequency of triggering storms, suggesting changes in the mechanical properties of hillslope sediment may drive this observation. The stabilisation of coseismically generated sediment greatly extends its residence time and may influence catchment sediment yields for centuries or millennia.

## Plain Language Summary

Earthquakes produce large volumes of sediment by triggering landslides in mountain ranges. After many earthquakes there is an order-of-magnitude increase in erosion rates, however this period of enhanced erosion is short lived. Understanding the processes which control the timespan of the elevated erosion rates and the rates at which they move sediment is vital for determining the continuing impact the earthquake has on a landscape. Using satellite imagery to map and track the movement of sediment after the 2008 Wenchuan earthquake we show that more than 88% (469 mega tonnes) of the sediment produced by the earthquake remains on the hillslope after a decade. Debris flows initiating in the landslide deposits are responsible for most of the erosion during this time. The frequency of these flows decreases rapidly after the earthquake indicating the sediment can stabilise rapidly. The stabilised sediment could reside in the mountain range for hundreds or thousands of years indicating that it could have a significant impact on erosion rates and landscape evolution.

## 1 Introduction

Large, continental earthquakes can produce thousands of coseismic landslides eroding several cubic kilometres of sediment from the hillslopes of tectonically active mountain ranges (Keefer, 2002; Malamud et al., 2004). Coseismic landsliding potentially accounts for over 50% of long term erosion rates in these mountains (G. Li et al., 2014, 2017; Marc, Hovius, & Meunier, 2016; Marc, Hovius, Meunier, et al., 2016). Understanding how earthquakes affect the evolution of landscapes requires a consideration of both the direct impact of the landslides on hillslopes and how the erosion or storage of the sediment impacts the evolution of the channel network (Campforts et al., 2020; Egholm et al., 2013). Coseismic landslides reduce the relief of steep hillslopes and can alter the size of drainage basins via erosion of basin ridges (Dahlquist et al., 2018; Schmidt & Montgomery, 1995). Furthermore landslide deposits contribute to debris flow generation (Fan, Scaringi, Korup, et al., 2019) and provide tools or cover for abrading/protecting the bedrock channels altering the evolution of upland rivers (Egholm et al., 2013; Turowski & Rickenmann, 2009; Yanites et al., 2010). Long term storage of the coseismically generated sediment can dampen the isostatic response of an earthquake (Densmore et al., 2012) or reduce the bedrock erosion of future earthquakes (Francis et al., 2020; G. Li et al., 2014; Marc, Hovius, & Meunier, 2016; Stolle et al., 2019). Therefore, to fully incorporate earthquakes into models of landscape evolution we must understand the processes and timescales by which coseismically generated sediment is exported from orogens. Key to this aim is fully understanding and quantifying the erosional processes which mobilise coseismically generated sediment following earthquakes.

Following large earthquakes it is typical (though not ubiquitous; (Tolorza et al., 2019)) to see an order-of-magnitude increase in sediment discharge in orogen draining rivers (Dadson et al., 2004; Hovius et al., 2000, 2011; Pain & Bowler, 1973; J. Wang et al., 2015). However, this period of elevated erosion is generally short lived, typically lasting less than a decade, resulting in significant, but unquantified, volumes of sediment remaining in the orogen after sediment discharges have returned to previous levels. As many coseismic landslides occur in bedrock much of the sediment within their deposits is too coarse to be transported by suspension resulting in aggradation of channels for decades after an earthquake (Koi et al., 2008; Pearce & Watson, 1986; Vanmaercke et al., 2017). This coarse sediment must be transported by bedload processes and is likely to remain in the landscape for hundreds of years. Empirical estimates of bedload transport estimate that the sediment from the 1999 Chi Chi earthquake in Taiwan could take 250-600 years to be fully evacuated from the landscape (Yanites et al., 2010). Detailed dating and mapping of the Pokhara region in Nepal also suggests river system can rework sediment from large earthquakes for several hundred years (Schwanghart et al., 2016; Stolle et al., 2017, 2019).

Alongside the residence time of sediment in the fluvial system, we must also consider possible storage of sediment on the hillslopes. Small landslide deposits can be deposited on the hillslope far from the river or deposited in channels which lack the discharge to consistently erode them (G. Li et al., 2016; Pearce & Watson, 1986; Roback et al., 2018). Landslides disconnected from the channel network cannot be actively reworked by undercutting and therefore must be eroded into the channel network by diffusive processes or stochastically by debris flows, which could significantly increase their residence times (Fan, Scaringi, Korup, et al., 2019; Vanmaercke et al., 2014; S. Zhang & Zhang, 2017). Attempting to include connectivity in dynamic models of sediment transport is difficult due to the rates and initiation mechanisms of these processes being

unknown in many locations. However, simple statistical numerical modelling suggests that unconnected landslide deposits could extend the period of time impacted by the earthquake by hundreds or thousands of years (Croissant et al., 2019; Francis et al., 2020).

Satellite imagery with high spatial and temporal resolution allows for the monitoring of large areas of mountain ranges. These can be used to generate multi-temporal landslide inventories after major earthquakes to understand the spatio-temporal evolution of post-seismic mass wasting processes (Kinney et al., 2021; Marc et al., 2015; Chenxiao Tang et al., 2016; S. Zhang & Zhang, 2017). Multi-temporal inventories can provide a link between long term sedimentary (Stolle et al., 2019) and short term suspended sediment discharge records (Lin et al., 2008) by helping to identify the key sediment transport processes. Here we use multitemporal landslide and channel width inventories of the epicentral area of the 2008  $M_w$  7.9 Wenchuan earthquake to generate the first sediment budget of a large earthquake. These 2 inventories, combined with a literature review, allow us to account for the sources, transport and storage of sediment produced during and in the 10 years following the earthquake (Dietrich et al., 1982; Hinderer, 2012). We use this sediment budget to determine the key sediment transport processes in the post-seismic landscape and to pose questions about the long-term evolution of the epicentral area.

## 1.2 The Longmen Shan and the 2008 $M_w$ 7.9 Wenchuan earthquake

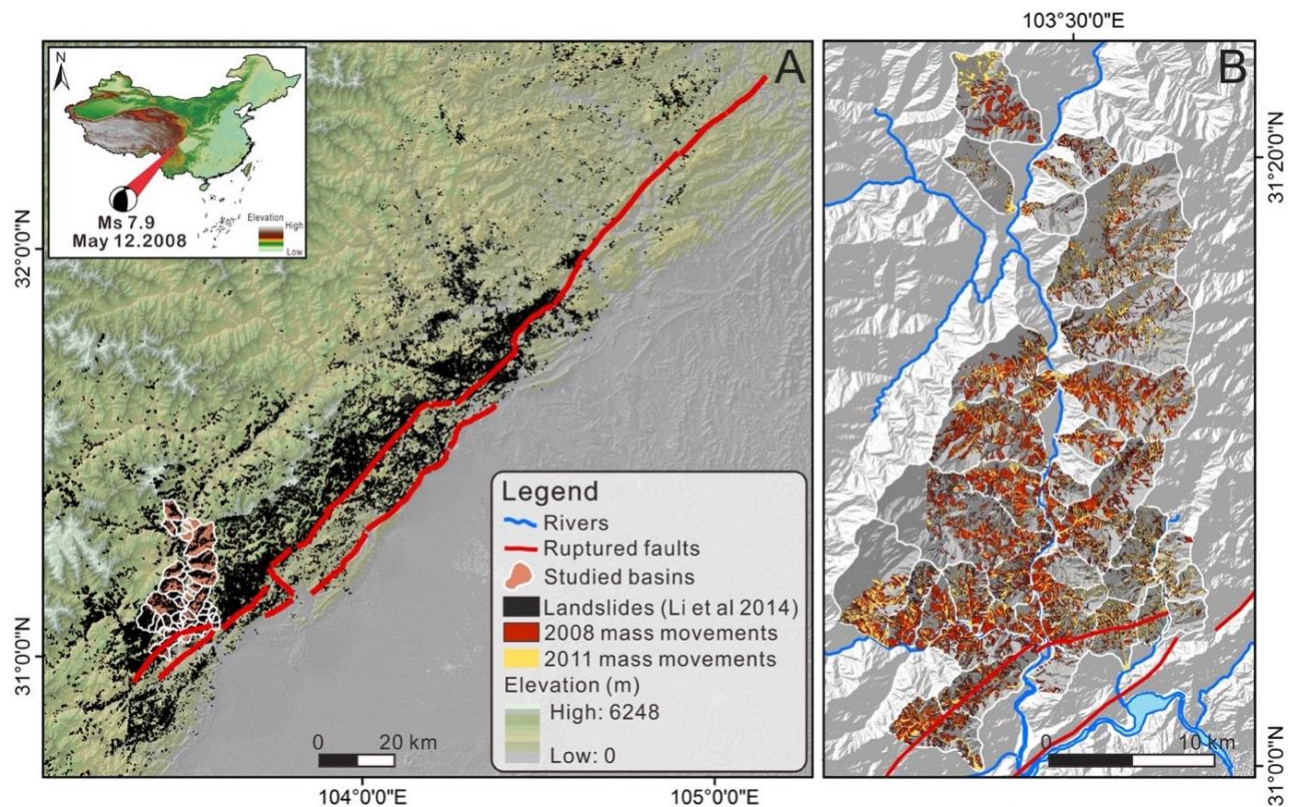


**Figure 1.** A) A map of the area affected by the Wenchuan Earthquake. The coseismic landslides mapped by Li et al., 2014 are shown in black while our studied catchments are shown in red with white outlines. The surface expression of the ruptured faults is shown as thick red lines. B) A focus on our study area with the mapped coseismic and the post-seismic mass movements of

2008-2011 mapped in red and yellow respectively. The main trunk of the Min Jiang is highlighted in blue and all the mapped sub-catchments flow into this river. An example of a mapped catchment can be found in Figure S1.

On 12 May 2008 the Wenchuan region, Sichuan, China, was shaken by a  $M_w 7.9$  earthquake with both thrust and dextral strike-slip components. The earthquake occurred along the Longmen Shan thrust zone, which separates the Longmen Shan mountain range from the Sichuan Basin, and ruptured 2 major faults (Figure 1) (Densmore et al., 2010; Liu-Zeng et al., 2009). The earthquake triggered more than 60,000 landslides across an area of 35,000 km<sup>2</sup> (Huang & Fan, 2013; G. Li et al., 2014) making it one of the most erosive earthquakes on record (Marc, Hovius, Meunier, et al., 2016). Coseismic landsliding is found in the greatest densities on the fault's hanging wall close to the traces of the ruptured faults with areal densities of up to 9.6% (Dai et al., 2011). Areas around the fault zone have weaker rock strength than expected of fresh bedrock (Gallen et al., 2015) and higher denudation rates than the rest of the landscape, suggesting frequent earthquakes have conditioned the area resulting in rapid erosion rates (G. Li et al., 2017).

The Longmen Shan is one of the steepest mountain ranges in the world, the frontal range rapidly increases in elevation from 500 to 4000 m over distances of just 50 km (Kirby & Ouimet, 2011). The mountain range is the eastern margin of the Tibetan Plateau in an area of complex tectonic and geodynamic activity (Burchfiel et al., 2008; Hubbard & Shaw, 2009; Royden et al., 2008). The high mountain peaks are dissected by deeply incised valleys and gorges of the rivers draining the mountain range (Densmore et al., 2007; Kirby & Ouimet, 2011). The Min Jiang, the major river draining the epicentral area, is bordered with several layers of terraces which record the long-term uplift and incision of the area (Godard et al., 2010). The main trunk of the river has a characteristic width of 100 m while many of the tributary catchments which drain into the river in the epicentral region of the earthquake are significantly smaller (Figure 2A). Rainfall is highly variable across the mountain range with the highest annual precipitation (800 – 1200 mm) found right on the mountain front (Guo et al., 2016). Rainfall and river discharge also vary temporally, the monsoon season between May and October is responsible for the majority of the rainfall and discharge (J. Wang et al., 2015). Mass movements are common in the Longmen Shan due to the steep hillslopes and high frequency of intense rain storms in the mountain range (Ouimet et al., 2007, 2009).

Following the earthquake, coseismic landslide sediment immediately was immediately eroded and reworked by the fluvial system. Suspended sediment discharges in the Min Jiang, and other rivers, increased by an order of magnitude (J. Wang et al., 2015), while the concentrations of cosmogenic <sup>10</sup>Be in detrital sediment dramatically declined (W. Wang et al., 2017; West et al., 2014). On average these records show that sediment transport has or is returning rapidly to pre-earthquake levels in the years since. However, there is significant variation in this pattern which is primarily linked to the landslide density in individual catchments. Catchments with higher landslide densities and more frequent large rainstorms tend to produce larger and longer lasting increases in sediment discharge (J. Wang et al., 2015; W. Wang et al., 2017). These increases seem to be unaffected by the volume of sediment connected to channel network. Here connection defines the location of the landslide deposit in relation to the channel network. Any landslide deposit that is deposited into the channel network is deemed connected. Around 40% of the total



coseismic landslide sediment volume is connected to the channel network but suspended sediment discharge remains high even in locations with low connectivity (G. Li et al., 2016). The lack of a correlation between suspended sediment discharge and connectivity could be an indicator of the high mobility of fine sediment immediately after the earthquake.

The most striking indicator of the earthquake significantly impacting the sediment transport rates of the area is the occurrence of huge (mobilising  $>10^6$  m<sup>3</sup> of sediment) debris flows (C. Tang et al., 2012). These are some of the largest debris flows ever observed and have occurred with frequencies rarely seen elsewhere (Korup, 2012). The debris flows occurred in the smaller tributary catchments of the Min Jiang where high landslide densities are common and significant aggradation of the channel bed is observed (S. Zhang & Zhang, 2017) (Figure 2b). These large debris flows are likely to be single largest part of the stochastic sediment cascades (Bennett et al., 2014; S. Zhang & Zhang, 2017). Understanding these events in the context of other smaller processes in a sediment budget is important to determine the likely future evolution of risk and landscape processes in the region.

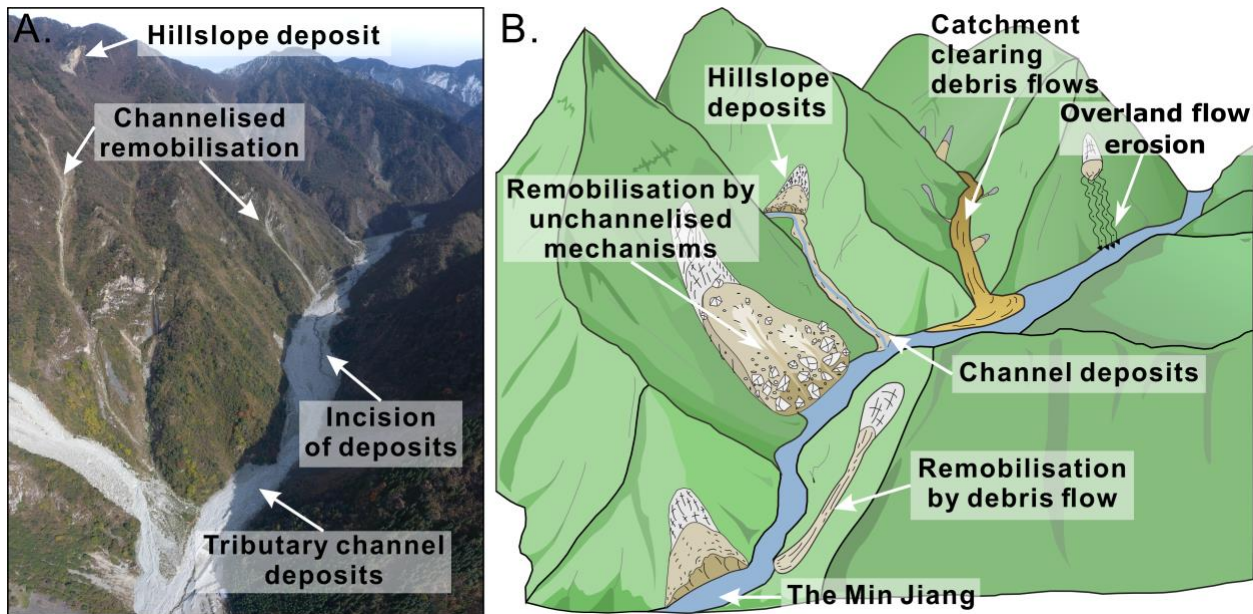


**Figure 2.** A) Drone image of a sub-catchment of the Min Jiang, taken in October 2019. The main sediment storage types are highlighted as well as the visible signs of sediment transport. B) A conceptual cartoon of the Min Jiang following the earthquake. The main sediment transport processes are represented along with their sources and sinks.

## 2 Materials and Methods

### 2.1 Study area

Our sediment budget is focused upon the Min Jiang as it passes through the epicentral region of the Wenchuan earthquake (Figure 1). The study area is made up of 28 sub-catchments which discharge directly into the main trunk of the Min Jiang (Figure 1B). This area was one of the

most strongly affected by the earthquake, with widespread landsliding dramatically hampering recovery efforts (Chuan Tang & Van Westen, 2018). Thousands of landslides were triggered on the steep hillslopes with an aerial density of up to 9.6% (Dai et al., 2011). This loose sediment was eroded during monsoon seasons of 2008, 2010, 2013, and 2019. The largest debris flows blocked the Min Jiang flooding the recovering Yingxiu (Chuan Tang et al., 2011).

This area offers an excellent opportunity to study the sediment dynamics of a post seismic landscape due to the high density of landsliding and rapid erosion rates. The suspended sediment load in the Min Jiang suggests erosion rates increased by an order of magnitude while the nearby Zipingpu reservoir offers an opportunity to analyse the impact of the earthquake on a local sink (J. Wang et al., 2015; F. Zhang et al., 2019). Field observations indicate that despite the high erosion rates large volumes of sediment still remain in the area trapped on the hillslopes and within the channel deposits of the tributary sub-catchments.

The study area is well served by high resolution satellites with frequent cloud free imagery allowing for multiple repeat surveys of the hillslopes and channels. We use these images to construct our multi-temporal mass movement and channel width inventories. We then use previously published databases of large debris flow events (Fan, Scaringi, Domènech, et al., 2019) and suspended sediment discharge (J. Wang et al., 2015) and field records of overland flow erosion to produce a complete sediment budget (Fusun et al., 2013).

## 2.2 Construction of the sediment budget

For all tributary catchments in our study area, we systematically calculated the mass budget for all of the hillslope and channel processes present in these catchments. We identified the mass of sediment transported by each processes using a combination of multi-temporal mapping using high resolution satellite imagery or from values reported in the literature, each calculation is described in detail below. We assume that minimal sediment was present in the landscape prior to the earthquake, an observation supported by the observations of narrow channels and large areas of exposed bedrock in pre-earthquake images. The primary source of post-earthquake sediment are co-seismic mass movements (landslides and debris flows) and minor post-seismic mass movements. Debris flows are identified in the satellite imagery by their characteristic long and thin shape sometimes with visible levees, while landslides are wide with no channelisation visible.

Sediment generated on hillslopes can either be stored on the hillslope or be transferred into and stored in the tributary channels. There are many processes that contribute to the transfer of sediment within the tributary catchments (Figure 2). Coseismic landslide debris can be eroded by overland flow, which we estimate based on observations in the literature scaled to the study area. Coseismic landslides can be eroded by subsequent mass movement processes that may, in some cases generate debris flows. We term the general processes of erosion by mass movement as remobilisation and further designate this into channelised and unchannelised forms (Fan et al. 2018). Channelised remobilisations are triggered within previous mass movement material and are long and thin and are likely to have created debris flows. Unchannelised remobilisations were polygons without any clear channelisation and can be formed by shallow landsliding within a previous deposit or may be produced by a dense, impossible to resolve from the imagery, rill network (Figure 2, Figure S2). We constrain the mass of landslides and unchannelised



remobilisations using area-volume scaling relationships, however no consistent scaling relationship exists for debris flows. The volume of debris flows is calculated as the residual after constraining the volumes of all other processes in the mass balance calculation. Once material has been eroded from hillslopes, it can either be stored within the tributary catchments or enter the Min Jiang. We use changes in channel deposit width observed on the satellite imagery and assumptions about channel shape to estimate changes in channel storage within the tributary catchments.

A number of processes can transfer mass from tributary catchments into the Min Jiang. Numerous extremely large, catchment clearing, debris flows occurred during the monsoons of 2008, 2010, 2013, and 2019. These created fans in the Min Jiang whose volume was measured and published (Fan, Scaringi, Domènech, et al., 2019; Yang et al., 2021). Additionally fluvial processes can erode channel material, the bedload component of this can be estimated from changes in storage within the tributary channels, while suspended sediment loads have been estimated in the literature.

To compute our estimates of the total sediment budget of the 10 years following the Wenchuan earthquake we used a Monte Carlo simulation framework. This framework allowed us to constrain the considerable uncertainty of each process and the final budget. For each epoch within our study period we ran 10,000 simulations within which we produced an estimate of the volume of sediment mobilised by each process by sampling from their uncertainty. We describe the processes and their uncertainty in detail in the section below.

### 2.3. Sediment sources: Mass movements

We constrained the volume and mass of sediment generated within each epoch of our study with a multi-temporal mass movement inventory. This inventory is an adapted version of the inventory described in (Fan, Scaringi, Domènech, et al., 2019), here we will briefly describe the methodology used to generate this inventory and key alterations.

The inventory is derived from orthorectified satellite (and some aerial) imagery of 6 different years after the earthquake (Table S1). The 2011 image provided coverage of the entire area in high resolution and hence was chosen as the geo-referencing base for the study. Each image was orthorectified using the Pix4D software before detailed checks were employed to ensure there were no major rectifying errors between the inventories (Williams et al., 2018). The timing of these images defines the epochs of our sediment budgets; 2008 (coseismic budget), 2009-2011, 2012-2013, 2014-2015, 2016-2018.

In each image we visually mapped any new mass movements (mass movements originating in previously undisturbed hillslope material) along with any remobilisation within the mass movements mapped in a previous image. All mass movements were mapped as polygons which covered the entire area of the mass movement, no effort was made to separate the source and deposition areas. New mass movements were primarily identified via changes in vegetation and supported by identification of channels, rills, and movement of boulders. Remobilisations were mapped by comparing different images and identifying changes within previously mapped mass movements regardless of vegetation cover (Figure S2). These changes could be the formation of rill networks, debris flows or landslide scars, or the clear movement of boulders. Any mass

movement which intersected with a previously mapped mass movement was classified as a remobilisation, as it likely entrained previously deposited sediment. This classification system differs from the ‘activity level’ used in the original inventory where landslides are classified by the area of the polygon not covered by vegetation (Fan, Scaringi, Domènech, et al., 2019; Chenxiao Tang et al., 2016). Our mapping scheme allowed us to directly map the area of the remobilisation which we then used as the base of our mass movement sediment budget.

Within this mapping scheme we classified four processes in each epoch; landslides, debris flows, unchannelised remobilisations, and channelised remobilisations using the definitions of Fan et al. (2018) (Figure S1). This classification was determined visually based upon the shape of the mapped polygons. Debris flows polygons are long and thin possibly with visible levees while landslides are wide with no channelisation visible. We also classified the remobilisation polygons using a similar scheme, however as less data exists for these processes, we used more generalised terms. Channelised remobilisation polygons are triggered within previous mass movement material and are long and thin similar to debris flows. Unchannelised remobilisations were polygons without any clear channelisation and can be formed by shallow landsliding within a previous deposit or may be produced by a dense, impossible to resolve from the imagery, rill network (Figure 2, Figure S2). Within our sediment budget we combine channelised remobilisation and debris flows into the single term debris flows as we cannot estimate their volumes or masses separately.

The mapped surface area of a landslide is converted into an estimate of deposit volume using an empirical area – volume scaling relationship ( $V = \alpha A^Y$  where  $V$  is the volume of the landslide,  $A$  is its scar area and  $\alpha$  and  $Y$  are empirical parameters). To ensure the runout of a landslide, which can significantly increase the surface area of a landslide without altering its runout, does not affect the resulting volume this calculation should be done on the mapped scar area of the landslide. However, we did not separate scar area and runout when mapping the mass movements within our inventory. To estimate the scar areas of our mapped landslides we used the correction methodology developed by (Marc et al., 2018, 2019). This correction assumes the scar area is elliptical and uses an estimated ellipse aspect ratio, derived from the area and perimeter of the mass movement, to determine the area of the scar. We apply this correction to all landslides and unchannelised remobilisations in our inventory. To determine the impact of this correction on estimations of landsliding volume we calculate the total volume for both the corrected and non-corrected volumes.

In our field location, the area – volume scaling parameters as only a small number of landslides have had their volumes recorded. Many global and some local scaling parameters have been published by there is significant variation between these studies (Larsen et al., 2010; G. Li et al., 2014). In order to constrain the impact this uncertainty has on estimating the volume of sediment generated by landslides we estimated the total landsliding volume using the Monte Carlo simulation methodology proposed by Li et al. (2014). Within each of our sediment budget Monte Carlo runs we randomly sampled from each of six sets of scaling parameters (Table 1) to generate an estimate of the total landsliding volume for that epoch. For each simulation we randomly choose six  $\alpha$  and  $Y$  values for each polygon (1 for each scaling parameter set) by assuming a uniform distribution within the uncertainty stated in Table 1. We then summed the total landsliding volume estimated by each scaling parameter set and reported the median

volume across these values for use in that budget simulation run. Finally, we then calculated the median and standard deviation of all 10,000 simulations to determine the uncertainty of the total landsliding volume.

Reference	$\text{Log}_{10}\alpha$	$Y$	Total Coseismic Volume ( $\text{km}^3$ )	Total Corrected Coseismic Volume ( $\text{km}^3$ )	Total Post-seismic Volume ( $\text{km}^3$ )	Total Corrected Post-seismic Volume ( $\text{km}^3$ )
(Larsen et al., 2010)	-0.836 $\pm 0.015$	1.332 $\pm 0.005$	0.6 ( $\pm 0.001$ )	0.2 ( $\pm 0.0004$ )	0.003 ( $\pm 0.00003$ )	0.0007 ( $\pm 0.00001$ )
(Larsen et al., 2010)	-0.73 $\pm 0.06$	1.35 $\pm 0.01$	1 ( $\pm 0.001$ )	0.2 ( $\pm 0.002$ )	0.004 ( $\pm 0.0001$ )	0.001 ( $\pm 0.00003$ )
(Larsen et al., 2010)	-0.59 $\pm 0.03$	1.36 $\pm 0.01$	1 ( $\pm 0.007$ )	0.4 ( $\pm 0.002$ )	0.007 ( $\pm 0.0001$ )	0.001 ( $\pm 0.00003$ )
(Guzzetti et al., 2009)	-1.131	1.45 $\pm 0.009$	1 ( $\pm 0.004$ )	0.3 ( $\pm 0.001$ )	0.004 ( $\pm 0.00007$ )	0.0009 ( $\pm 0.00002$ )
(Parker et al., 2011)	-0.974 $\pm 0.366$	1.388 $\pm 0.087$	2 ( $\pm 0.1$ )	0.4 ( $\pm 0.04$ )	0.006 ( $\pm 0.002$ )	0.001 ( $\pm 0.0004$ )
(G. Li et al., 2014)	-0.995 $\pm 0.366$	1.392 $\pm 0.087$	2 ( $\pm 0.1$ )	0.4 ( $\pm 0.04$ )	0.006 ( $\pm 0.002$ )	0.001 ( $\pm 0.0004$ )
Combined			1 (-0.6/+0.5)	0.3 ( $\pm 0.1$ )	0.005 ( $\pm 0.002$ )	0.001 ( $\pm 0.0005$ )

**Table 1.** The results of the Monte Carlo Simulations. Each set of parameters is run 10,000 times and combined to produce an overall estimate of total volume and uncertainty. Coseismic volume includes all landslides that are mapped in the 2008 image while the post-seismic volume includes all new landslides mapped after this year. No other process was included. Total corrected volumes refers to the area derived from the scar area correction derived by (Marc et al., 2018).

#### 2.4 Sediment transfer and temporary storage – Tributary channel deposits

We mapped the width of the channel deposits on average every 200m along the tributary channels, from the head of the tributary to its confluence with the Min Jiang for the 17 largest catchments in our study area. For each epoch the resolution of the satellite imagery was 2.5m and the length of time between catchment surveys varied from 1 – 3 years. The width of the channel deposit was defined as the length of a straight line from one edge of the non-vegetated sediment bed of a channel to the other (Figure S3). Each cross section was mapped in section of the valley free from landslide deposits which impinged directly onto the drainage network so that only sediment within the channel bed was included in the survey.

To convert the mapped widths into volumes we assumed a cross sectional area of the channel using rectangular, trapezoidal or circular segments (Figure S3). Varying between the volume estimates produced by using these shapes in each Monte Carlo run provides an estimate of uncertainty. For each cross sectional area we estimated the depth of the tributary channel deposits from the mapped widths using an empirical relationship derived by (Moody & Troutman, 2002). To calculate the area of trapezoid cross sections we also required an estimate

of the bank angle of the tributary catchment. Using a buffer of 100 meters from the mapped widths, the bank angles varied between 25 and 35 degrees. We varied the bank angle between this range 10,000 times for each width and calculated the mean area. The volume of the channel material was calculated by integrating across the distances between the surveys.

Changes in the volume stored within channels were measured via changes in the mapped channel widths between epochs. If the width expanded we assumed there had been a depositional episode and so subtracted the previous estimate of stored sediment from the new larger volume to determine the increase in storage. If the width had not changed between the epochs we assumed that no deposition had occurred. Instead, we mapped the width of the active channel which was incising through the channel deposits, estimated the volume of sediment mobilised by this incision, and assumed that it enters the Min Jiang. The mapped active channel (identified by the presence of water) is likely a result of debris flow activity and fluvial reworking of the sediment and therefore this process is termed incision within our sediment budget.

As the 17 catchments were not surveyed at the same time the number of surveys and the time between them differs for each catchment. Therefore, to determine a sediment budget for the entire study area for the epochs of the mass movement sediment budget, we averaged the sediment budget of each catchment. For each epoch of the catchment we divided the change in sediment storage by the time between the surveys (units of  $\text{m}^3/\text{yr.}$ ). This averaged rate was then combined with the results of the rest of the catchments to produce an average change in storage estimate for the entire area. Finally, we multiplied the average rate by the number of surveyed catchments (units of  $\text{m}^3$ ) and across each epoch to allow us to compare the 2 sediment budgets.

## 2.5 Sediment transfer – Remobilisations and debris flows

To determine an estimate of the sediment transferred from the hillslopes to the channel network we calculated the volume of sediment remobilised from the landslide deposits and how much was deposited into the channel network.

The area-volume scaling relationship for remobilisation processes is poorly constrained, particularly if they are channelised. For unchannelised remobilisations we used the same area – volume scaling methodology as described in section 2.3. However unlike coseismic landslides which can originate in bedrock, the volume of a remobilisation is limited by the depth of the deposit it originates in. Therefore, if a particular combination of area-volume scaling parameters produced an average unchannelised remobilisation deposit depth greater than the average depth of coseismic landslide deposits ( $\sim 7\text{m}$ ) the simulation is discarded. This threshold ensures the volume of sediment of the unchannelised remobilisations is constrained by the volume of sediment available on the hillslopes. However, we found that for the final epoch (2016-2018) it was not possible to determine the volume of the unchannelised remobilisation using the parameter set in Table 1. Therefore, we used another set of scaling parameters, the shallow landsliding parameters determined by Larsen et al. (2010) ( $\text{Log}_{10}\alpha = -0.836 \pm 0.015$ ,  $Y = 1.145 \pm 0.008$ ), and a series of average depths ranging from 0.2 – 1.9 meters.

The volumes of debris flows and channelised remobilisations are harder to quantify as flowing mass movements gain volume through entrainment of loose sediment along their runout path.

While some estimates of the volume of sediment entrained by debris flows do exist (Ma et al., 2017) these are poorly constrained. Further, in order to ensure mass is balanced we calculate the volume of debris flows and channelised remobilisations by differencing the other components of the balance. Debris flows can only mobilise sediment from the hillslopes into the channel deposits, therefore a threshold was imposed which prevented the estimate from becoming negative and removing sediment from the tributary channel deposits.

To determine the volume of sediment entering the tributary channel deposits or Min Jiang from remobilisations we defined a hillslope/channel drainage area threshold. If the maximum drainage area of an unchannelised remobilisation polygon is greater than the threshold, the calculated volume of the polygon is assigned to the channel network. The threshold was derived from a threshold based channel extraction algorithm in the software LSDTopoTools (Mudd et al., 2020). An initial estimate of a threshold was derived from mapping likely channel head locations in satellite imagery. However, due to the uncertainty in this approach we produced a second threshold from the LSDTopoTools generated channel network. This final threshold was derived from the median drainage area of the first order channels (700,000m<sup>2</sup>). If a remobilisation shapefile had a drainage area greater than this threshold it is assigned to the tributary channel deposits. Any polygon which had a maximum drainage area greater than that of a Strahler stream order 6 channel was automatically assigned to the Min Jiang rather than the tributary channel deposits, termed coseismic Min Jiang deposits or remobilised into the Min Jiang in our budget.

Within this budget we assume only remobilisations and debris flows can deposit sediment into tributary channel deposits. No undercutting of landslide deposits by the tributary channels was identified in either field observations or imagery, instead most landslides were remobilised by hillslope processes. The tributary channels are small and do not have the transport capacity to mobilise the coarse sediment of the deposits. Therefore, in our sediment budget all landslides are initially added to the hillslope deposit store unless they are deposited directly into the Min Jiang. Debris flows by contrast can deposit directly into the tributary channel deposits (or the Min Jiang) as their greater mobility allows them to travel along the channel before depositing. To produce an estimate of sediment mobilised into the tributary channel deposits during the earthquake we applied the runout correction methodology to the coseismic debris flow polygons and added the resulting volumes to the tributary channel deposits. As we do not consider any potential sediment gained during the runout of the debris flow, our initial estimate of the volume within the tributary channel deposits is likely to be an underestimation.

## 2.6 Sediment transfer – Overland flow erosion

The loose sediment on the hillslopes, particularly fine-grained sediment can be mobilised by runoff into the tributary channel deposits. This process occurs on small scales and is unlikely to be visible on satellite imagery. We estimated the volume of sediment mobilised by this process by scaling the field measurements performed by Fusun et al (2013). They deployed sediment traps to record the volume of sediment leaving landslides over a single monsoon period. We extrapolated them, assuming a constant erosion rate, across the active bare area of the mass movements for each time step. We do not consider the impact the variability of rainfall may have on this process, thus our estimates are could be an overestimation considering the strong

monsoon which occurred during the original study (Fusun et al., 2013; Shen et al., 2020). The uncertainty reported in our mass balanced is as reported in the source material.

## 2.7 Sediment export – Catchment clearing debris flows

Catchment clearing debris flows are large debris flows which evacuate sediment from the hillslopes and tributary channels and deposit it directly into the Min Jiang (Figure S2). These debris flows produce large depositional fans which intersect directly with the main trunk of the Min Jiang. A database of the volumes of these depositional fans was compiled from technical reports and papers by (Fan, Scaringi, Domènech, et al., 2019). As uncertainty data was unavailable for most of the events, we assumed an uncertainty of  $\pm 50\%$  of the reported volume. Catchment clearing debris flows mobilise sediment from both the hillslope and tributary channel deposits. They can be triggered by landsliding on the hillslopes, run off within the channel, or the merging of multiple smaller debris flows (P. Cui et al., 2013; C. Tang et al., 2012). Debris flows can also bulk significantly along their runout with sediment from along the channel bed producing total deposit volumes at least an order of magnitude greater than their initiation volumes (Horton et al., 2019). As the majority of the sediment entrained by its runout is redeposited before the debris flow reaches the Min Jiang, we assume the recorded volumes of catchment clearing debris flows are equally made up of hillslope and tributary channel deposits.

## 2.8 Sediment export – Suspended sediment

Suspended sediment is an indicator of fluvial export of sediment in a catchment area and thus we include it as a process within our budget. The suspended sediment load does not include bedload transport into the Min Jiang so we have attempted to estimate this separately (incision). We estimated the mass of coseismic sediment mobilised by this process using the records of sediment discharge of the Min Jiang and other rivers reported by Wang et al. (2015). Wang et al. (2015) compiled yearly records of suspended sediment discharge for a number of sampling stations on rivers draining the epicentral area of the earthquake. For each station they reported pre (2006 – 2007) and post (2008-2012) earthquake sediment discharges and the mass of the landslides upstream of the station. We used this data to determine a simple linear trend ( $r^2 = 0.46$ ) between the mass of landsliding upstream of a station and the increase in yearly suspended sediment discharge. We used this trend to estimate the suspended sediment transport related to the earthquake in our area. As we do not have any data covering the study area beyond 2012, we simply assume that the suspended sediment discharge remains constant. This is likely to be an overestimation as many studies have indicated that suspended sediment discharge decreases to its background rate within a decade of the earthquake (Hovius et al., 2011; J. Wang et al., 2015; W. Wang et al., 2017). Uncertainty in our values is derived from the uncertainty within our coseismically generated sediment mass estimates (Table 1). We assumed all sediment mobilised by this process originated within the tributary channel deposits.

## 2.9 Converting volume in mass

To convert our sediment volume budgets into mass budgets we must multiply the volumes by a density. As the density of the sediment with our study (and how it may change between stores) is



not known we use a further Monte Carlo simulation for the conversion. We randomly sample from the range of volumes mobilised by each process and multiple this by a random density. For the density we used an estimate typical of alluvial sediment 2000 ( $\pm 300$ ) kg/m<sup>3</sup>.

## 4 Results

### 4.1 Full post-earthquake sediment budget

In the study area, we mapped a total of 15,130 mass movements (8,830 coseismic and 6,300 post-seismic) across the study period (Fig 1B). These mass movements generated a total volume of 0.3 ( $\pm 0.1$ ) km<sup>3</sup> of sediment which has an estimated mass of 531 ( $\pm 280$ ) Mega tonnes. 99% of the sediment was generated coseismically, indicating any post-seismic enhancement of landsliding is not a significant contributor to post-seismic sediment discharges. Of the sediment that was mobilised from the hillslopes after the earthquake, less than 1% was from new post-seismic mass movements suggesting the increase in sediment discharge records is almost exclusively driven by remobilisation of coseismic sediment. Less than 18%, (4.7 Mt;  $\pm 2.6$ ), of the sediment deposited into the Min Jiang was from coseismic landslide material deposited directly into the main trunk of the river (Table 2). The majority of sediment deposited into the Min Jiang after the earthquake travels through the tributary channels. Nearly all of the post-seismic sediment that enters the Min Jiang transits tributary channels (Figure 3). Our observations demonstrate that the post-earthquake sediment cascade includes multiple steps within hillslopes and tributary channels prior to entering the Min Jiang.

At the end of the decade long study, 88% of the sediment generated during and after the earthquake remains on hillslopes. 6% is deposited in the tributary channels and the final 6% has entered the Min Jiang (Table 2). Of the sediment that was deposited on the hillslopes during the earthquake 90% remains. 80% (44 Mt;  $\pm 14$ ) of the sediment remobilised from the hillslopes is deposited into the tributary channel deposits where it requires further remobilisation before it is evacuated from the orogen.

The sediment mass mobilised by debris flows peaks between 2009 – 2011 before declining sharply after 2015. This appears to be offset from peaks in the frequency of channelised remobilisations and new debris flows (Table S2) immediately after the earthquake. This discrepancy could reflect a change in the size frequency of remobilisations or due to an underestimation of the sediment entering the channel network. This underestimation could be due to a lack of imagery before 2008 to estimate the volume of sediment within the channels prior to the earthquake. We observe a large number of smaller debris flows in during the first epoch, which would support change in size frequency. We estimate that debris flows mobilise 22.9 ( $\pm 10.6$ ) Mt of sediment after the earthquake, most of which enters the tributary channel deposits making them the most significant sediment remobilisation process.

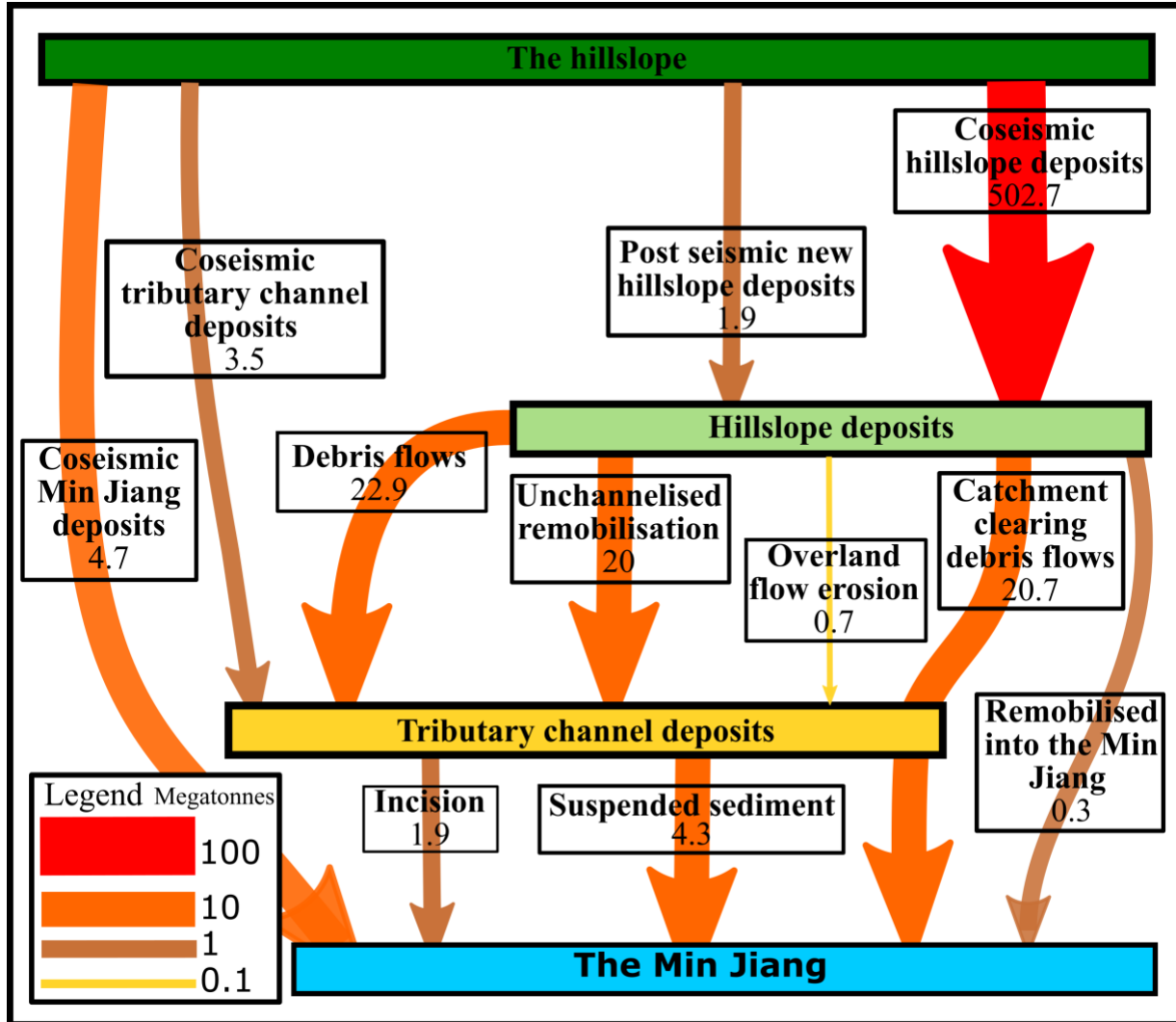


**Figure 3.** The sediment budget of the Wenchuan Earthquake. The width and colour of each arrow indicates the magnitude of the sediment moved by the process between the stores. Each arrow is labelled with the process it represents with the median mass estimate. The uncertainty of each measurement can be found in Table 2. Catchment clearing debris flows erode sediment from both hillslope and tributary channel deposits and therefore is represented by an arrow passing through the tributary channel deposits in a single motion.

Large catchment clearing debris flows are the major process depositing sediment into the Min Jiang accounting for 76% (27.2;  $\pm 13.8$  Mt) of the sediment deposited into the river after the earthquake. Debris flows (both small channelised remobilisations and large catchment clearing flows) dominate the sediment budget accounting for 69% (40.7;  $\pm 14$  Mt) of all sediment mobilised after the earthquake. Fluvial processes (here represented by incision and suspended sediment), on the other hand, are only minor contributors to sediment transport over our study period.

552  
553

<b>Coseismic sediment budget</b>	<b>Mass (Mt)</b>	<b>Uncertainty (1 standard deviation, Mt)</b>	<b>%</b>
Coseismic hillslope deposits	520.7	274.5	98.1
Coseismic tributary channel deposits	3.5	1.8	0.7
Coseismic Min Jiang deposits	4.7	2.6	0.9
<b>Post-seismic new landslides and debris flows</b>			
Post-seismic new hillslope deposits	1.9	0.3	0.4
<b>Total sediment generated</b>	<b>530.8</b>	<b>279.2</b>	<b>100</b>
<b>Remobilisation of hillslope deposits</b>			
Debris flows	22.9	10.6	4.3
Unchannelised remobilisation	20	3.1	3.8
Into the Min Jiang	0.3	0.1	0.1
Overland flow erosion	0.7	0.2	0.1
<b>Remobilisation of channel deposits</b>			
Catchment clearing debris flows	20.7	10.9	3.9
Suspended sediment	4.3	1.7	0.8
Incision	1.9	1.2	0.4
<b>Stores</b>			
Hillslope deposits	468.3	288.2	88.2
Tributary channel deposits	30.5	16	5.8
Min Jiang	32	24.2	6

554 **Table 2.** The full sediment budget from figure 3 in table form. All values are rounded to 1  
555 decimal place. The percentage values are derived from the median value of each process and the  
556 total sediment generated.

#### 557 4.2 The sediment budget through time

558 Separating the budget into the 4 post-earthquake epochs (2009 – 2011, 2012 – 2013, 2014 –  
559 2015, and 2016 – 2018 inclusively) defined by the availability of satellite imagery allows us to  
560 analyse how the processes and overall discharge changes through time. We find that the total  
561 mass of sediment mobilised each year decreased by an order of magnitude from 13.3 ( $\pm 5.1$ ) —  
562 2.2 ( $\pm 0.9$ ) Mt/yr between 2011 and 2018 (Table 3). A total of 72.8 ( $\pm 28$ ) Mt of sediment (both

new and remobilised coseismically generated) is mobilised after the earthquake, 79% of which was mobilised during the first 5 years after the earthquake. The total sediment discharge decreases rapidly until 2015 after which it begins to level off suggesting it had begun to stabilise by the end of the study period.

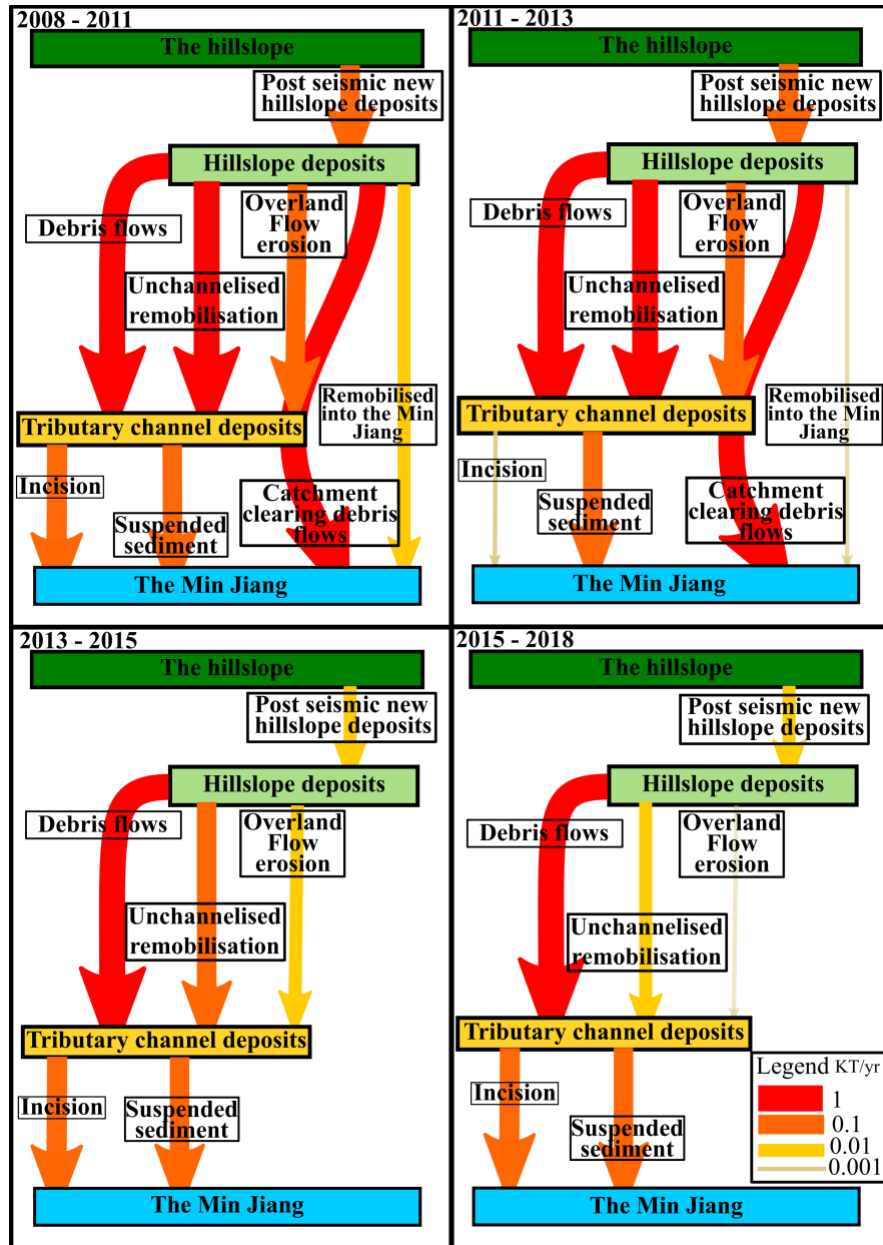


**Figure 4.** The sediment budget separated into 4 post-seismic epochs to show how the magnitude of the processes change through time. The thickness and colour of the arrow reflects the magnitude of the mass of sediment transferred by each process. If a transfer path becomes inactive during a particular epoch the arrow is removed from the diagram.

The rate at which the hillslope deposits are depleted decreases from  $9.0 (\pm 2.1)$  Mt/yr —  $1.4 (\pm 0.4)$  Mt/yr over our study period. For each epoch the volume of sediment produced by post-

seismic mass movements (new landsliding) is less than the volume remobilised from the hillslope deposits. This decrease in remobilisation rates coincides with the overall decrease in sediment discharge. As remobilisation of coseismic deposits continues to dominate the hillslope sediment discharge at the end of our study period, it is likely the overall discharge remains elevated above pre-earthquake levels.

Tributary channels have aggraded across the study period. The change in storage of the tributary channel deposits declines sharply after 2015 but still remains slightly positive. The major cause of the decrease in the tributary channel deposit budget seems to be due to a decrease in the volume of sediment being deposited within the channels. A slight increase in the volume of sediment leaving the deposits via incision is seen, however due to a lack of constraints we are not able to verify this pattern. If the deposition of sediment into the tributary channel deposits remains low it is likely the total volume of sediment stored will begin to decrease in the future.

Finally, we see an overall decrease in the sediment mass entering the Min Jiang across the study period. This coincides with changes in the frequency of large catchment clearing debris flows. Without these large flows the volume of sediment entering the Min Jiang decreases by almost a factor of 8, highlighting the importance of the largest mass movement events to evacuating the coseismic sediment from the Longmen Shan.

All units Mt/yr	2008 -2011	2011-2013	2013-2015	2015 - 2018
<b>Post-seismic new landslides and debris flows</b>				
Post-seismic new hillslope deposits	0.45 ( $\pm 0.07$ )	0.20 ( $\pm 0.02$ )	0.04	0.03 ( $\pm 0.01$ )
<b>Remobilisation of hillslope deposits</b>				
Debris flows	1.8 ( $\pm 1.3$ )	3.4 ( $\pm 1$ )	3.3 ( $\pm 0.8$ )	1.4 ( $\pm 0.5$ )
Unchannelised remobilisation	4.8 ( $\pm 0.7$ )	2.5 ( $\pm 0.3$ )	0.2 ( $\pm 0.02$ )	0.04 ( $\pm 0.01$ )
Into the Min Jiang	0.09 ( $\pm 0.02$ )	0.02	0	0
Overland Flow erosion	0.2 ( $\pm 0.1$ )	0.1 ( $\pm 0.01$ )	0.02	~0.0
<b>Remobilisation of Channel deposits</b>				
Catchment clearing debris flows	5 ( $\pm 2.6$ )	2.8 ( $\pm 1$ )	0	0
Suspended sediment	0.4 ( $\pm 0.1$ )	0.4 ( $\pm 0.1$ )	0.4 ( $\pm 0.1$ )	0.4 ( $\pm 0.1$ )
Incision	0.1 ( $\pm 0.07$ )	0.06 ( $\pm 0.03$ )	0.2 ( $\pm 0.1$ )	0.3 (0.2)

**Table 3.** The sediment budget separated into 4 epochs with each process quantified and averaged across the epoch. All units are in Mt/yr

## 5 Discussion

Our full sediment budget of the Wenchuan earthquake reveals that over 88% of the sediment produced by the earthquake remains on hillslopes 10 years after the earthquake. The majority of the coseismically generated sediment is mobilised by debris flows, either small flows which deposit sediment to the base of the hillslopes or rare large flows which can bypass the tributary channel deposits and mobilise sediment directly into the Min Jiang. Studies suggest that throughout geological history the frequency of events on the scale of the largest catchment clearing debris flows is significantly lower than we see after the earthquake (Korup, 2012). Therefore, the high frequency of catchment clearing debris flows we have observed is unlikely to be representative of the long-term trend and a decrease should be expected. Without these large catchment clearing debris flows most sediment will be stored and transported multiple times before it is evacuated from the mountain range. This pattern of remobilisation and deposition could be repeated multiple times likely extending the residence time of some sediment up to 100s if not 1000s of years.

As the residence time of sediment is so strongly affected by the largest and rarest of events it is important to observe the area of interest for the longest time possible. For example, within our study area there were no catchment clearing debris flows between 2013 and 2018 which dramatically decreases the sediment erosion rate of the area and would increase any estimates of residence time. However, in August 2019 a large storm (maximum intensity 28.5mm/hr) triggered 12 large catchment-clearing debris flows in our study area, some in catchments where no debris flow had occurred for over 5 years (Fan et al., 2020; Yang et al., 2021). Initial estimates of the volume of the debris flows suggested a total of  $1.9 \times 10^{-2}$  ( $\pm 3 \times 10^{-2}$ ) km<sup>3</sup> of sediment was transported by these events (Yang et al., 2021). Field investigation of the debris



flow deposits revealed that the majority of the sediment was deposited before it entered the Min Jiang, only a small volume was deposited as fans in the Min Jiang. As a crude estimate of the volume of sediment deposited into the Min Jiang, we can extrapolate the recorded volume of a single debris flow fan over all of the 12 flows. The deposition fan of the Manianping catchment has an estimated volume of  $7 \times 10^{-4} \text{ km}^3$  (Yang et al., 2021) assuming all 12 flows were of equal magnitude,  $8.4 \times 10^{-3} \text{ km}^3$  of sediment was deposited into the Min Jiang. Assuming a deposit density of  $2000 \text{ kg/m}^3$  we can estimate the impact of these flows upon our sediment budget, these flows potentially deposited 16.8 Mt of sediment into the Min Jiang more than tripling the final epoch's yearly average sediment mobilisation rate. Interestingly many of the 2019 catchment clearing debris flows occurred without significant remobilisation of hillslope deposits, indicating they removed sediment only from the tributary channel deposits (Fan et al., 2020). This activity could demonstrate a long-term shift in behaviour due to the stabilisation of the hillslope deposits in the epicentral area.

The frequency of sediment remobilisation from hillslopes has decreased since the earthquake. In the first epoch (2009–2011) of our budget we recorded 4296 remobilisation events, 1193 of which were channelised. However, in the final epoch (2016–2018) just 54 remobilisations were recorded (11 channelised). There is a similar decrease in the sediment mass mobilised by debris flows across this time, particularly in the final epoch. This rapid reduction in remobilisation cannot be related to exhaustion, and is most likely due to a stabilisation of hillslope deposits. This apparent stabilisation of hillslope deposits will extend the residence time of co-seismically generated sediment beyond that of what can be expected from rates recorded here. The reduction in debris-flow frequency we observe is also reported in other studies and after other earthquakes; rainfall intensity duration thresholds in the epicentral area have increased since the earthquake leading to indications of a stabilisation of the coseismically generated sediment taking place (Dahlquist & West, 2019; Fan et al., 2020; S. Zhang & Zhang, 2017).

The mechanisms behind the stabilisation of co-seismic mass movements not well understood through time, however there are several hypotheses which we will discuss here. The first is that colonisation of the landslide area by vegetation has increased the resistive strength of the landslide deposit. Depending on the triggering mechanism of the failure vegetation can stabilise the deposit in several ways. The canopy of vegetation can intercept the rainfall before it strikes the sediment reducing the local intensity and saturation state (McGuire et al., 2016; Wilkinson et al., 2002). While the trunks and stems of vegetation increase the roughness of the slope reducing the velocity of surface runoff and reducing shear stress of any overland flow. Vegetation can also increase the shear strength of the soil (T. C. Hales et al., 2009; Tristram C. Hales, 2018). A correlation between NDVI (Normalised Difference Vegetation Index) and the reduction in debris flow frequency have suggested that vegetation regrowth may be the mechanism by which this deposits stabilise (Fan, Domènech, et al., 2018; Yunus et al., 2020). However the first type of vegetation to colonise landslide areas are grasses and shrubs (Shen et al., 2020), most of which only have shallow and weak root structures which do not add significant strength to the sediment (Tristram C. Hales, 2018). The impact of vegetation may depend on triggering mechanism, as it is unlikely that grasses will have a large impact on debris flows triggered by shallow landsliding, but may impact surface runoff. While it is clear that there are many mechanisms by which sediment can be stabilised by vegetation, it is very unlikely that vegetation is solely responsible for the trends that we see after the earthquake.

Another mechanism for stabilisation is internal erosion of the hillslope deposits (Peng Cui et al., 2014; W. Hu et al., 2016; Wei Hu et al., 2017; S. Zhang & Zhang, 2017). It is hypothesised that fresh landslide deposits are highly permeable which allows water to pass through easily. As the water passes through the deposit it can entrain the fine sediment and move it through the deposit. As the fine sediment moves through the deposit it can induce small localised failures by blocking small pore spaces (Peng Cui et al., 2014). These small failures can coalesce to destabilise the deposit and cause a larger remobilisation of the sediment. If there is enough fluid within the failing deposit a debris flow can be formed. However, if no large-scale failure occurs many sections of the deposit will be in a fines depleted state. These areas will be more stable as they are more permeable and porous resulting in a greater hydraulic conductivity and possibly a greater internal friction angle (W. Hu et al., 2016; Wei Hu et al., 2017). The smaller failures may also compact the deposits which has also been shown to reduce the likelihood of failure in loose sediment (Chang et al., 2011; Iverson et al., 2000). However, there is minimal in situ evidence for this theory of preferential erosion of fine sediment.

Human activity may also have impacted sediment discharge due to engineering work within the channels (Fan, Juang, et al., 2018). This has the potential to significantly reduce the number of catchment-clearing debris flows in the area. However, the inaccessibility of the study catchments, means that population densities within them are low so minimal efforts have been made to stabilise most of the slope. Therefore while the frequency of channel clearing debris flows could be related to human activity, the stabilisation of the slopes cannot.

Finally, we need to consider the stochastic nature of mass movements. Mass movements are driven by stochastic rainfall events. Across our decadal observation window, we need to consider whether declines in mass-movement frequency are related to fewer triggering storm events. In the 10 years since the earthquake the most intense storm (1-hr intensity) occurred in 2013 (64.5 mm) with the second most intense occurring in 2017 (40.1 mm) (Shen et al., 2020). 2013 also experienced a similar amount of total precipitation to the 2011 but considerably less activity was recorded in 2013 across all scales (Fan, Scaringi, Domènech, et al., 2019; Fan, Scaringi, Korup, et al., 2019; F. Zhang et al., 2019). While the intensity of the monsoons vary year on year the frequency of observed sediment transport decreases (Table S2). There is no correlation between precipitation and mass movement frequency (or volume) following the earthquake.

The mass balance of first 10 years after the earthquake is dominated by mass movement events. Between 2013 and 2018 there are no catchment clearing debris flows and deposition into the Min Jiang more than halves (Table 3). In contrast the fluvial driven processes (termed incision in our budget) are more consistent in the rate of sediment export to the Min Jiang, but the rate is much smaller. Incision only accounts for 5% of the sediment entering the Min Jiang during the first decade after the earthquake. Further, fluvial erosion is only observed acting on sediment that has already been remobilised once by a mass movement process, there is little evidence that the tributary channels can erode the landslide deposits directly. The conclusion is that hillslope processes and their rates act as a primary control on the volume and timing sediment evacuation from the orogen. Fluvial erosion is likely slow at removing sediment from the tributary channel deposits due to the coarse nature of the stored sediment and low fluvial discharges. The coarse nature of the tributary channel deposits indicates that currently much of the sediment requires

debris flows, large floods or in situ break down of the boulders before it can be mobilised out of the orogen.

While we have few constraints sediment transport in the main trunk of the Min Jiang, the Zipingpu reservoir offers some insight into the sediment dynamics of the entire system. The Zipingpu reservoir is a man-made reservoir a few kilometres downstream of our study area. A borehole drilled in the centre of the reservoir by (F. Zhang et al., 2019) in 2016 identified that the earthquake had only had a slight impact on the sediment dynamics. No change in sedimentation rate was noticed, likely due to the distal location of the core relative to the mouth of the Min Jiang entering the reservoir, but a change in the chemistry and grain size was observed (F. Zhang et al., 2019). Grain size increased, possibly indicating the transport of coarser coseismic landslide derived sediment, and the Rb/Sr ratio decreased potentially due to an influx of unweathered (fresh landslide derived) sediment into the reservoir. Crucially while these signals were recognised immediately after the earthquake the biggest response was observed after the 2010 monsoon when significant volumes of coseismically generated sediment were deposited into the rivers draining into the reservoir by debris flows. This result agrees with our finding that debris flows are the major component in delivering sediment to the channel network. The borehole also suggests that the system is in a transport-limited state as grain size and total runoff is well correlated indicating the need for large events to mobilise much of the sediment (F. Zhang et al., 2019).

Our results indicate that co-seismic sediment likely has residence times of 1000's of years. Empirical and modelling studies suggest that the hillslopes will continue to be perturbed for at least another decade before returning to background levels (Chen et al., 2020; C. Li et al., 2020; Shen et al., 2020; Yunus et al., 2020). As this trend in declining activity is driven by stabilisation rather than exhaustion it is likely the residence time of the coseismically generated sediment will be significantly longer. Large earthquakes such as the Wenchuan earthquake have a return period of 500 – 4000 years and if coseismically generated sediment can remain being reworked for similar timescales it is likely erosion rates will be altered (Francis et al., 2020; G. Li et al., 2017). The large volumes of sediment on the hillslopes, which are on average steeper than the likely friction angle of sediment, will continue to be mobilised, albeit much slower than immediately after the earthquake. Erosion rates in the tributary channels and the Min Jiang are likely to be lowered if the bedload is not mobilised at rates significant enough to abrade the bed. Deposits of landslide derived sediment have been linked to knickpoints within the Longmen Shan indicating the region is prone to long periods of reduced erosion (Fan, Yunus, et al., 2019; Ouimet et al., 2007). If post-seismic reduction of erosion rates is frequent and wide spread, it is possible that the largest earthquakes may have a positive impact on the long-term mass balance of the mountain range despite the huge amount of erosion they initiate (Francis et al., 2020).

## 6 Conclusions

Here we have quantified the sediment cascade of the 10 years following the 2008 Wenchuan earthquake. Using a multitemporal landslide inventory, channel width surveys and constrained area – volume scaling relationships we tracked the evolution of 531 Mt of sediment. Of this sediment just 9% was deposited into the Min Jiang, the major orogen draining river of the study area. ~87% of the sediment deposited onto the hillslopes during the earthquake remains there waiting to be mobilised into the channel network. The key process in mobilising coseismic

sediment into the Min Jiang has been debris flows. The largest of these can deposit huge volumes of sediment from the tributary channels, overcoming the otherwise low transport capacity of the channels in these catchments. These large flows are highly stochastic and can occur after breaks of many years. Determining the frequency and magnitude of these events is crucial to estimating the residence time of the coseismically generated sediment. Finally, as large volumes of coseismically generated sediment can remain within the orogen for extended periods of time, their impact should be considered when modelling the long-term evolution of tectonically active mountain ranges.

## Acknowledgments, Samples, and Data

The authors declare no known conflicts of interest.

This work was funded by the Newton Fund, Natural Environmental Research Council, Economic and Social Research Council, and National Science Foundation for China grant, NE/N012240/1, the Funds for Creative Research Groups of China (Grant No. 41521002), and the Fund for International Cooperation (NSFC-RCUK\_NERC), Resilience to Earthquake-induced landslide risk in China (grant No. 41661134010). The authors would like to thank the team of mappers who helped put together the mass movement inventory on which this study was based. We would also like to thank A. Densmore and M. Singer for useful discussions which greatly enhanced this paper.

The original mass movement inventories upon which this study is based have been published (Fan et al, 2019) and can be found at <https://doi.org/10.5281/zenodo.1405489>.

The adapted mass movement inventories, the channel width inventories and the Python code used in this study can be found at <https://zenodo.org/record/5676154>

## References

- Bennett, G. L., Molnar, P., McArdell, B. W., & Burlando, P. (2014). A probabilistic sediment cascade model of sediment transfer in the Illgraben. *Water Resources Research*, 50(2), 1225–1244. <https://doi.org/10.1002/2013WR013806>
- Burchfiel, B. C., Royden, L. H., van der Hilst, R. D., Hager, B. H., Chen, Z., King, R. W., Li, C., Lü, J., Yao, H., & Kirby, E. (2008). A geological and geophysical context for the Wenchuan earthquake of 12 May 2008, Sichuan, People's Republic of China. *GSA Today*, 18(7), 4–11. <https://doi.org/10.1130/GSATG18A.1>
- Campforts, B., Shobe, C. M., Steer, P., Vanmaercke, M., Lague, D., & Braun, J. (2020). HyLands 1.0: A hybrid landscape evolution model to simulate the impact of landslides and landslide-derived sediment on landscape evolution. *Geoscientific Model Development*, 13(9), 3863–3886. <https://doi.org/10.5194/gmd-13-3863-2020>
- Chang, D. S., Zhang, L. M., Y., X., & Q., H. R. (2011). Field testing of erodibility of two landslide dams triggered by the 12 May Wenchuan earthquake. *Landslides*, 8(October 2009), 321–332. <https://doi.org/10.1007/s10346-011-0256-x>
- Chen, M., Tang, C., Xiong, J., Shi, Q. Y., Li, N., Gong, L. F., Wang, X. D., & Tie, Y. (2020). The long-term evolution of landslide activity near the epicentral area of the 2008 Wenchuan earthquake in China. *Geomorphology*, 367, 107317. <https://doi.org/10.1016/j.geomorph.2020.107317>
- Croissant, T., Steer, P., Lague, D., Davy, P., Jeandet, L., & Hilton, R. G. (2019). Seismic cycles,

earthquakes, landslides and sediment fluxes: Linking tectonics to surface processes using a reduced-complexity model. *Geomorphology*, 339, 87–103.  
<https://doi.org/10.1016/j.geomorph.2019.04.017>

Cui, P., Zhou, G. G. D., Zhu, X. H., & Zhang, J. Q. (2013). Scale amplification of natural debris flows caused by cascading landslide dam failures. *Geomorphology*, 182(August 2010), 173–189. <https://doi.org/10.1016/j.geomorph.2012.11.009>

Cui, Peng, Guo, C. xu, Zhou, J. wen, Hao, M. hui, & Xu, F. gang. (2014). The mechanisms behind shallow failures in slopes comprised of landslide deposits. *Engineering Geology*, 180, 34–44. <https://doi.org/10.1016/j.enggeo.2014.04.009>

Dadson, S. J., Hovius, N., Chen, H., Dade, W. B., Lin, J.-C., Hsu, M.-L., Lin, C.-W., Horng, M.-J., Chen, T.-C., Milliman, J., & Stark, C. P. (2004). Earthquake-triggered increase in sediment delivery from an active mountain belt. *Geology*, 32(8), 733.  
<https://doi.org/10.1130/G20639.1>

Dahlquist, M. P., & West, A. J. (2019). Initiation and Runout of Post-Seismic Debris Flows: Insights From the 2015 Gorkha Earthquake. *Geophysical Research Letters*, 46(16), 9658–9668. <https://doi.org/10.1029/2019GL083548>

Dahlquist, M. P., West, A. J., & Li, G. (2018). Landslide-driven drainage divide migration. *Geology*, 46(5), 403–406. <https://doi.org/https://doi.org/10.1130/G39916.1>

Dai, F. C., Xu, C., Yao, X., Xu, L., Tu, X. B., & Gong, Q. M. (2011). Spatial distribution of landslides triggered by the 2008 Ms 8.0 Wenchuan earthquake, China. *Journal of Asian Earth Sciences*, 40(4), 883–895. <https://doi.org/10.1016/j.jseaes.2010.04.010>

Densmore, A. L., Ellis, M. A., Li, Y., Zhou, R., Hancock, G. S., & Richardson, N. (2007). Active tectonics of the Beichuan and Pengguan faults at the eastern margin of the Tibetan Plateau. *Tectonics*, 26(4), 1–17. <https://doi.org/10.1029/2006TC001987>

Densmore, A. L., Li, Y., Richardson, N. J., Zhou, R., Ellis, M., & Zhang, Y. (2010). The role of late quaternary upper-crustal faults in the 12 may 2008 Wenchuan earthquake. *Bulletin of the Seismological Society of America*, 100(5 B), 2700–2712.  
<https://doi.org/10.1785/0120090294>

Densmore, A. L., Parker, R. N., Rosser, N. J., De Michele, M., Yong, L., Runqiu, H., Whadcoat, S., & Petley, D. N. (2012). Reply to “Isostasy can’t be ignored.” *Nature Geoscience*, 5(2), 83–84. <https://doi.org/10.1038/ngeo1385>

Dietrich, W. E., Dunne, T., Humphrey, N. F., & Reid, L. M. (1982). Construction of sediment budgets for drainage basins. *Workshop on Sediment Budgets and Routing in Forested Drainage Basins: Proc.*, 5–23.

Egholm, D. L., Knudsen, M. F., & Sandiford, M. (2013). Lifespan of mountain ranges scaled by feedbacks between landsliding and erosion by rivers. *Nature*, 498(7455), 475–478.  
<https://doi.org/10.1038/nature12218>

Fan, X., Domènech, G., Scaringi, G., Huang, R., Xu, Q., Hales, T. C., Dai, L., Yang, Q., & Francis, O. (2018). Spatio-temporal evolution of mass wasting after the 2008 Mw 7.9 Wenchuan Earthquake revealed by a detailed multi-temporal inventory. *Landslides*, 15(September), 2325–2341. <https://doi.org/10.1007/s10346-018-1054-5>

- Fan, X., Juang, C. H., Wasowski, J., Huang, R., Xu, Q., Scaringi, G., van Westen, C. J., & Havenith, H. B. (2018). What we have learned from the 2008 Wenchuan Earthquake and its aftermath: A decade of research and challenges. *Engineering Geology*, 241(May), 25–32. <https://doi.org/10.1016/j.enggeo.2018.05.004>
- Fan, X., Scaringi, G., Domènech, G., Yang, F., Guo, X., Dai, L., He, C., Xu, Q., & Huang, R. (2019). Two multi-temporal datasets that track the enhanced landsliding after the 2008 Wenchuan earthquake. *Earth System Science Data*, 11(1), 35–55. <https://doi.org/10.5194/essd-11-35-2019>
- Fan, X., Scaringi, G., Korup, O., West, A. J., van Westen, C. J., Tanyas, H., Hovius, N., Hales, T. C., Jibson, R. W., Allstadt, K. E., Zhang, L., Evans, S. G., Xu, C., Li, G., Pei, X., Xu, Q., & Huang, R. (2019). Earthquake-Induced Chains of Geologic Hazards: Patterns, Mechanisms, and Impacts. *Reviews of Geophysics*. <https://doi.org/10.1029/2018RG000626>
- Fan, X., Yunus, A. P., Jansen, J. D., Dai, L., Strom, A., & Xu, Q. (2019). Comment on ‘Gigantic rockslides induced by fluvial incision in the Diexi area along the eastern margin of the Tibetan Plateau’ by Zhao et al. (2019) *Geomorphology* 338, 27–42. *Geomorphology*, xxxx, 106963. <https://doi.org/10.1016/j.geomorph.2019.106963>
- Fan, X., Yunus, A. P., Scaringi, G., Catani, F., Subramanian, S. S., Xu, Q., & Huang, R. (2020). Rapidly evolving controls of landslides after a strong earthquake and implications for hazard assessments. *Geophysical Research Letters*, 33(0), 2–31. <https://doi.org/10.1029/2020GL090509>
- Francis, O. R., Hales, T. C., Hobley, D. E. J., Fan, X., Horton, A. J., Scaringi, G., & Huang, R. (2020). The impact of earthquakes on orogen-scale exhumation. *Earth Surface Dynamics*, 8(3), 579–593. <https://doi.org/10.5194/esurf-8-579-2020>
- Fusun, S., Jinniu, W., Tao, L., Yan, W., Haixia, G., & Ning, W. (2013). Effects of different types of vegetation recovery on runoff and soil erosion on a Wenchuan earthquake-triggered landslide, China. *Journal of Soil and Water Conservation*, 68(2), 138–145. <https://doi.org/10.2489/jswc.68.2.138>
- Gallen, S. F., Clark, M. K., & Godt, J. W. (2015). Coseismic landslides reveal near-surface rock strength in a highrelief, tectonically active setting. *Geology*, 43(1), 11–14. <https://doi.org/10.1130/G36080.1>
- Godard, V., Lavé, J., Carcaillet, J., Cattin, R., Bourlès, D., & Zhu, J. (2010). Spatial distribution of denudation in Eastern Tibet and regressive erosion of plateau margins. *Tectonophysics*, 491(1–4), 253–274. <https://doi.org/10.1016/j.tecto.2009.10.026>
- Guo, X., Cui, P., Li, Y., Ma, L., Ge, Y., & Mahoney, W. B. (2016). Intensity-duration threshold of rainfall-triggered debris flows in the Wenchuan Earthquake affected area, China. *Geomorphology*, 253, 208–216. <https://doi.org/10.1016/j.geomorph.2015.10.009>
- Guzzetti, F., Ardizzone, F., Cardinali, M., Rossi, M., & Valigi, D. (2009). Landslide volumes and landslide mobilization rates in Umbria, central Italy. *Earth and Planetary Science Letters*, 279(3–4), 222–229. <https://doi.org/10.1016/j.epsl.2009.01.005>
- Hales, T. C., Ford, C. R., Hwang, T., Vose, J. M., & Band, L. E. (2009). Topographic and ecologic controls on root reinforcement. *Journal of Geophysical Research: Solid Earth*, 114(3), 1–17. <https://doi.org/10.1029/2008JF001168>



- 886 Hales, Tristram C. (2018). Modelling biome-scale root reinforcement and slope stability. *Earth*  
 887 *Surface Processes and Landforms*, 43(10), 2157–2166. <https://doi.org/10.1002/esp.4381>
- 888 Hinderer, M. (2012). From gullies to mountain belts: A review of sediment budgets at various  
 889 scales. *Sedimentary Geology*, 280, 21–59. <https://doi.org/10.1016/j.sedgeo.2012.03.009>
- 890 Horton, A. J., Hales, T. C., Ouyang, C., & Fan, X. (2019). Identifying post-earthquake debris  
 891 flow hazard using Massflow. *Engineering Geology*, 258.  
 892 <https://doi.org/10.1016/j.enggeo.2019.05.011>
- 893 Hovius, N., Meunier, P., Lin, C. W., Chen, H., Chen, Y. G., Dadson, S., Horng, M. J., & Lines,  
 894 M. (2011). Prolonged seismically induced erosion and the mass balance of a large  
 895 earthquake. *Earth and Planetary Science Letters*, 304(3–4), 347–355.  
 896 <https://doi.org/10.1016/j.epsl.2011.02.005>
- 897 Hovius, N., Stark, C. P., Hao-Tsu, C., & Jiun-Chuan, L. (2000). Supply and Removal of  
 898 Sediment in a Landslide-Dominated Mountain Belt: Central Range, Taiwan. *The Journal of*  
 899 *Geology*, 108(1), 73–89. <https://doi.org/10.1086/314387>
- 900 Hu, W., Dong, X. J., Xu, Q., Wang, G. H., van Asch, T. W. J., & Hicher, P. Y. (2016). Initiation  
 901 processes for run-off generated debris flows in the Wenchuan earthquake area of China.  
 902 *Geomorphology*, 253, 468–477. <https://doi.org/10.1016/j.geomorph.2015.10.024>
- 903 Hu, Wei, Scaringi, G., Xu, Q., Pei, Z., Van Asch, T. W. J., & Hicher, P. Y. (2017). Sensitivity of  
 904 the initiation and runout of flowslides in loose granular deposits to the content of small  
 905 particles: An insight from flume tests. *Engineering Geology*, 231(July), 34–44.  
 906 <https://doi.org/10.1016/j.enggeo.2017.10.001>
- 907 Huang, R., & Fan, X. (2013). The landslide story. *Nature Geoscience*, 6(5), 325–326.  
 908 <https://doi.org/10.1038/ngeo1806>
- 909 Hubbard, J., & Shaw, J. H. (2009). Uplift of the Longmen Shan and Tibetan plateau, and the  
 910 2008 Wenchuan ( $M = 7.9$ ) earthquake. *Nature*, 458(7235), 194–197.  
 911 <https://doi.org/10.1038/nature07837>
- 912 Iverson, R. M., Reid, M. E., Iverson, N. R., LaHusen, R. G., Logan, M., Mann, J. E., & Brien, D.  
 913 L. (2000). Acute sensitivity of landslide rates to initial soil porosity. *Science*, 290(5491),  
 914 513–516. <https://doi.org/10.1126/science.290.5491.513>
- 915 Keefer, D. K. (2002). Investigating landslides caused by earthquakes - A historical review.  
 916 *Surveys in Geophysics*, 23(6), 473–510. <https://doi.org/10.1023/A:1021274710840>
- 917 Kinsey, M. E., Rosser, N. J., Robinson, T. R., Densmore, A. L., Shrestha, R., Pujara, D. S.,  
 918 Oven, K. J., Williams, J. G., & Swirad, Z. M. (2021). Evolution of coseismic and post-  
 919 seismic landsliding after the 2015  $M_w 7.8$  Gorkha earthquake, Nepal. *Journal of*  
 920 *Geophysical Research: Earth Surface*. <https://doi.org/10.1029/2020jf005803>
- 921 Kirby, E., & Ouimet, W. (2011). Tectonic geomorphology along the eastern margin of Tibet:  
 922 insights into the pattern and processes of active deformation adjacent to the Sichuan Basin.  
 923 *Geological Society, London, Special Publications*, 353(1), 165–188.  
 924 <https://doi.org/10.1144/SP353.9>
- 925 Koi, T., Hotta, N., Ishigaki, I., Matuzaki, N., Uchiyama, Y., & Suzuki, M. (2008). Prolonged  
 926 impact of earthquake-induced landslides on sediment yield in a mountain watershed: The

- 927 Tanzawa region, Japan. *Geomorphology*, 101(4), 692–702.  
 928 <https://doi.org/10.1016/j.geomorph.2008.03.007>
- 929 Korup, O. (2012). Earth's portfolio of extreme sediment transport events. *Earth-Science*  
 930 *Reviews*, 112(3–4), 115–125. <https://doi.org/10.1016/j.earscirev.2012.02.006>
- 931 Larsen, I. J., Montgomery, D. R., & Korup, O. (2010). Landslide erosion controlled by hillslope  
 932 material. *Nature Geoscience*, 3(4), 247–251. <https://doi.org/10.1038/ngeo776>
- 933 Li, C., Wang, M., Liu, K., & Coulthard, T. J. (2020). Landscape evolution of the Wenchuan  
 934 earthquake-stricken area in response to future climate change. *Journal of Hydrology*, 590,  
 935 125244. <https://doi.org/10.1016/j.jhydrol.2020.125244>
- 936 Li, G., West, A. J., Densmore, A. L., Hammond, D. E., Jin, Z., Zhang, F., Wang, J., & Hilton, R.  
 937 G. (2016). Connectivity of earthquake-triggered landslides with the fluvial network:  
 938 Implications for landslide sediment transport after the 2008 Wenchuan earthquake. *Journal*  
 939 *of Geophysical Research: Earth Surface*, 121(4), 703–724.  
 940 <https://doi.org/10.1002/2015JF003718>
- 941 Li, G., West, A. J., Densmore, A. L., Jin, Z., Parker, R. N., & Hilton, R. G. (2014). Seismic  
 942 mountain building: Landslides associated with the 2008 Wenchuan earthquake in the  
 943 context of a generalized model for earthquake volume balance. *Geochemistry, Geophysics,*  
 944 *Geosystems*, 15(4), 833–844. <https://doi.org/10.1002/2013GC005067>
- 945 Li, G., West, A. J., Densmore, A. L., Jin, Z., Zhang, F., Wang, J., Clark, M., & Hilton, R. G.  
 946 (2017). Earthquakes drive focused denudation along a tectonically active mountain front.  
 947 *Earth and Planetary Science Letters*, 472, 253–265.  
 948 <https://doi.org/10.1016/j.epsl.2017.04.040>
- 949 Lin, G.-W., Chen, H., Hovius, N., Horng, M.-J., Dadson, S., Meunier, P., & Lines, M. (2008).  
 950 Effects of earthquake and cyclone sequencing on landsliding and fluvial sediment transfer  
 951 in a mountain catchment. *Earth Surface Processes and Landforms*, 33(9), 1354–1373.  
 952 <https://doi.org/10.1002/esp.1716>
- 953 Liu-Zeng, J., Zhang, Z., Wen, L., Tapponnier, P., Sun, J., Xing, X., Hu, G., Xu, Q., Zeng, L.,  
 954 Ding, L., Ji, C., Hudnut, K. W., & van der Woerd, J. (2009). Co-seismic ruptures of the 12  
 955 May 2008, Ms8.0 Wenchuan earthquake, Sichuan: East-west crustal shortening on oblique,  
 956 parallel thrusts along the eastern edge of Tibet. *Earth and Planetary Science Letters*, 286(3–  
 957 4), 355–370. <https://doi.org/10.1016/j.epsl.2009.07.017>
- 958 Ma, C., Wang, Y., Hu, K., Du, C., & Yang, W. (2017). Rainfall intensity–duration threshold and  
 959 erosion competence of debris flows in four areas affected by the 2008 Wenchuan  
 960 earthquake. *Geomorphology*, 282, 85–95. <https://doi.org/10.1016/j.geomorph.2017.01.012>
- 961 Malamud, B. D., Turcotte, D. L., Guzzetti, F., & Reichenbach, P. (2004). Landslides,  
 962 earthquakes, and erosion. *Earth and Planetary Science Letters*, 229(1–2), 45–59.  
 963 <https://doi.org/10.1016/j.epsl.2004.10.018>
- 964 Marc, O., Behling, R., Andermann, C., Turowski, J. M., Illien, L., Roessner, S., & Hovius, N.  
 965 (2019). Long-term erosion of the Nepal Himalayas by bedrock landsliding: the role of  
 966 monsoons, earthquakes and giant landslides. *Earth Surface Dynamics*, 7, 107–128.  
 967 <https://doi.org/10.5194/esurf-2018-69>

- 968 Marc, O., Hovius, N., & Meunier, P. (2016). The mass balance of earthquakes and earthquake  
 969 sequences. *Geophysical Research Letters*, 43(8), 3708–3716.  
 970 <https://doi.org/10.1002/2016GL068333>
- 971 Marc, O., Hovius, N., Meunier, P., Gorum, T., & Uchida, T. (2016). A seismologically  
 972 consistent expression for the total area and volume of earthquake-triggered landsliding.  
 973 *Journal of Geophysical Research: Earth Surface*, 121(4), 640–663.  
 974 <https://doi.org/10.1002/2015JF003732>
- 975 Marc, O., Hovius, N., Meunier, P., Uchida, T., & Hayashi, S. (2015). Transient changes of  
 976 landslide rates after earthquakes. *Geology*, 43(10), 883–886.  
 977 <https://doi.org/10.1130/G36961.1>
- 978 Marc, O., Stumpf, A., Malet, J., Gosset, M., Uchida, T., & Chiang, S. (2018). Initial insights  
 979 from a global database of rainfall-induced landslide inventories : the weak influence of  
 980 slope and strong influence of total storm rainfall. *Earth Surface Dynamics*, 6, 903–922.  
 981 <https://doi.org/https://doi.org/10.5194/esurf-6-903-2018>
- 982 McGuire, L. A., Kean, J. W., Staley, D. M., Rengers, F. K., & Wasklewicz, T. A. (2016).  
 983 Constraining the relative importance of raindrop- and flow-driven sediment transport  
 984 mechanisms in postwildfire environments and implications for recovery time scales.  
 985 *Journal of Geophysical Research: Earth Surface*, 121(11), 2211–2237.  
 986 <https://doi.org/10.1002/2016JF003867>
- 987 Moody, J. A., & Troutman, B. M. (2002). Characterization of the spatial variability of channel  
 988 morphology. *Earth Surface Processes and Landforms*, 27(12), 1251–1266.  
 989 <https://doi.org/10.1002/esp.403>
- 990 Mudd, S. M., Clubb, F., & Hurst, M. (2020). *LSDtopotools/LSDTopoTools2: LSDTopoTools2*  
 991 *v0.3*. <https://doi.org/10.5281/ZENODO.3769703>
- 992 Ouimet, W. B., Whipple, K. X., & Granger, D. E. (2009). Beyond threshold hillslopes: Channel  
 993 adjustment to base-level fall in tectonically active mountain ranges. *Geology*, 37(7), 579–  
 994 582. <https://doi.org/10.1130/G30013A.1>
- 995 Ouimet, W. B., Whipple, K. X., Royden, L. H., Sun, Z., & Chen, Z. (2007). The influence of  
 996 large landslides on river incision in a transient landscape: Eastern margin of the Tibetan  
 997 Plateau (Sichuan, China). *Bulletin of the Geological Society of America*, 119(11–12), 1462–  
 998 1476. <https://doi.org/10.1130/B26136.1>
- 999 Pain, C. F., & Bowler, J. M. (1973). Denudation following the November 1970 earthquake.  
 1000 *Zeitschrift Fur Geomorphologie*, 18, 92–104.
- 1001 Parker, R. N., Densmore, A. L., Rosser, N. J., De Michele, M., Li, Y., Huang, R., Whadcoat, S.,  
 1002 & Petley, D. N. (2011). Mass wasting triggered by the 2008 Wenchuan earthquake is  
 1003 greater than orogenic growth. *Nature Geoscience*, 4(7), 449–452.  
 1004 <https://doi.org/10.1038/ngeo1154>
- 1005 Pearce, A. J., & Watson, A. J. (1986). Effects of earthquake-induced landslides on sediment  
 1006 budget and transport over a 50-yr period. *Geology*, 14, 52–55.
- 1007 Roback, K., Clark, M. K., West, A. J., Zekkos, D., Li, G., Gallen, S. F., Chamlagain, D., & Godt,  
 1008 J. W. (2018). The size, distribution, and mobility of landslides caused by the 2015 Mw7.8

- 1009 Gorkha earthquake, Nepal. *Geomorphology*, 301, 121–138.  
 1010 <https://doi.org/10.1016/j.geomorph.2017.01.030>
- 1011 Royden, L. H., Burchfiel, B. C., & van der Hilst, R. D. (2008). The Geological Evolution of the  
 1012 Tibetan Plateau. *Science*, 321(5892), 1054–1058. <https://doi.org/10.1126/science.1155371>
- 1013 Schmidt, K. M., & Montgomery, D. R. (1995). Limits to Relief. *Science*, 270(5236), 617–620.  
 1014 <https://doi.org/10.1126/science.270.5236.617>
- 1015 Schwanghart, W., Bernhardt, A., Stolle, A., Hoelzmann, P., Adhikari, B. R., Andermann, C.,  
 1016 Tofelde, S., Merchel, S., Rugel, G., Fort, M., & Korup, O. (2016). Repeated catastrophic  
 1017 valley infill following medieval earthquakes in the Nepal Himalaya. *Science*, 351(6269),  
 1018 147–150. <https://doi.org/10.1126/science.aac9865>
- 1019 Shen, P., Zhang, L. M., Fan, R. L., Zhu, H., & Zhang, S. (2020). Declining geohazard activity  
 1020 with vegetation recovery during first ten years after the 2008 Wenchuan earthquake.  
 1021 *Geomorphology*, 352, 106989. <https://doi.org/10.1016/j.geomorph.2019.106989>
- 1022 Stolle, A., Bernhardt, A., Schwanghart, W., Hoelzmann, P., Adhikari, B. R., Fort, M., & Korup,  
 1023 O. (2017). Catastrophic valley fills record large Himalayan earthquakes, Pokhara, Nepal.  
 1024 *Quaternary Science Reviews*, 177, 88–103. <https://doi.org/10.1016/j.quascirev.2017.10.015>
- 1025 Stolle, A., Schwanghart, W., Andermann, C., Bernhardt, A., Fort, M., Jansen, J. D., Wittmann,  
 1026 H., Merchel, S., Rugel, G., Adhikari, B. R., & Korup, O. (2019). Protracted river response  
 1027 to medieval earthquakes. *Earth Surface Processes and Landforms*, 44(1), 331–341.  
 1028 <https://doi.org/10.1002/esp.4517>
- 1029 Tang, C., Van Asch, T. W. J., Chang, M., Chen, G. Q., Zhao, X. H., & Huang, X. C. (2012).  
 1030 Catastrophic debris flows on 13 August 2010 in the Qingping area, southwestern China:  
 1031 The combined effects of a strong earthquake and subsequent rainstorms. *Geomorphology*,  
 1032 139–140(August 2010), 559–576. <https://doi.org/10.1016/j.geomorph.2011.12.021>
- 1033 Tang, Chenxiao, Van Westen, C. J., Tanyas, H., & Jetten, V. G. (2016). Analysing post-  
 1034 earthquake landslide activity using multi-temporal landslide inventories near the epicentral  
 1035 area of the 2008 Wenchuan earthquake. *Natural Hazards and Earth System Sciences*,  
 1036 16(12), 2641–2655. <https://doi.org/10.5194/nhess-16-2641-2016>
- 1037 Tang, Chuan, & Van Westen, C. J. (2018). *Atlas of Wenchuan-Earthquake Geohazards: Analysis*  
 1038 *of co-seismic and post-seismic Geohazards in the area affected by the 2008 Wenchuan*  
 1039 *Earthquake*. Science Press.  
 1040 [https://issuu.com/ceesvanwesten/docs/atlas\\_of\\_wenchuan\\_earthquake\\_geohaz](https://issuu.com/ceesvanwesten/docs/atlas_of_wenchuan_earthquake_geohaz)
- 1041 Tang, Chuan, Zhu, J., Ding, J., Cui, X., Chen, L., & Zhang, J. (2011). Catastrophic debris flows  
 1042 triggered by a 14 August 2010 rainfall at the epicenter of the Wenchuan earthquake.  
 1043 *Landslides*, 8(4), 485–497. <https://doi.org/10.1007/s10346-011-0269-5>
- 1044 Tolorza, V., Mohr, C. H., Carretier, S., Serey, A., Sepúlveda, S. A., Tapia, J., & Pinto, L. (2019).  
 1045 Suspended Sediments in Chilean Rivers Reveal Low Postseismic Erosion After the Maule  
 1046 Earthquake (Mw 8.8) During a Severe Drought. *Journal of Geophysical Research: Earth*  
 1047 *Surface*, 124(6), 1378–1397. <https://doi.org/10.1029/2018JF004766>
- 1048 Turowski, J. M., & Rickenmann, D. (2009). Tools and cover effects in bedload transport  
 1049 observations in the Pitzbach, Austria. *Earth Surface Processes and Landforms*, 34(1), 26–

- 1050 37. <https://doi.org/10.1002/esp.1686>
- 1051 Vanmaercke, M., Ardizzone, F., Rossi, M., & Guzzetti, F. (2017). Exploring the effects of  
1052 seismicity on landslides and catchment sediment yield: An Italian case study.  
1053 *Geomorphology*, 278, 171–183. <https://doi.org/10.1016/j.geomorph.2016.11.010>
- 1054 Vanmaercke, M., Obreja, F., & Poesen, J. (2014). Seismic controls on contemporary sediment  
1055 export in the Siret river catchment, Romania. *Geomorphology*, 216, 247–262.  
1056 <https://doi.org/10.1016/j.geomorph.2014.04.008>
- 1057 Wang, J., Jin, Z., Hilton, R. G., Zhang, F., Densmore, A. L., Li, G., & Joshua West, A. (2015).  
1058 Controls on fluvial evacuation of sediment from earthquake-triggered landslides. *Geology*,  
1059 43(2), 115–118. <https://doi.org/10.1130/G36157.1>
- 1060 Wang, W., Godard, V., Liu-Zeng, J., Scherler, D., Xu, C., Zhang, J., Xie, K., Bellier, O.,  
1061 Ansberque, C., & de Sigoyer, J. (2017). Perturbation of fluvial sediment fluxes following  
1062 the 2008 Wenchuan earthquake. *Earth Surface Processes and Landforms*, 42(15), 2611–  
1063 2622. <https://doi.org/10.1002/esp.4210>
- 1064 West, A. J., Hetzel, R., Li, G., Jin, Z., Zhang, F., Hilton, R. G., & Densmore, A. L. (2014).  
1065 Dilution of  $^{10}\text{Be}$  in detrital quartz by earthquake-induced landslides: Implications for  
1066 determining denudation rates and potential to provide insights into landslide sediment  
1067 dynamics. *Earth and Planetary Science Letters*, 396, 143–153.  
1068 <https://doi.org/10.1016/j.epsl.2014.03.058>
- 1069 Wilkinson, P. L., Anderson, M. G., & Lloyd, D. M. (2002). An integrated hydrological model for  
1070 rain-induced landslide prediction. *Earth Surface Processes and Landforms*, 27(12), 1285–  
1071 1297. <https://doi.org/10.1002/esp.409>
- 1072 Williams, J. G., Rosser, N. J., Kincey, M. E., Benjamin, J., Oven, K. J., Densmore, A. L.,  
1073 Milledge, D. G., Robinson, T. R., Jordan, C. A., & Dijkstra, T. A. (2018). Satellite-based  
1074 emergency mapping using optical imagery: Experience and reflections from the 2015 Nepal  
1075 earthquakes. *Natural Hazards and Earth System Sciences*, 18(1), 185–205.  
1076 <https://doi.org/10.5194/nhess-18-185-2018>
- 1077 Yang, F., Fan, X., Siva Subramanian, S., Dou, X., Xiong, J., Xia, B., Yu, Z., & Xu, Q. (2021).  
1078 Catastrophic debris flows triggered by the 20 August 2019 rainfall, a decade since the  
1079 Wenchuan earthquake, China. *Landslides*, October 2020. [https://doi.org/10.1007/s10346-](https://doi.org/10.1007/s10346-021-01713-6)  
1080 021-01713-6
- 1081 Yanites, B. J., Tucker, G. E., Mueller, K. J., & Chen, Y.-G. (2010). How rivers react to large  
1082 earthquakes: Evidence from central Taiwan. *Geology*, 38(7), 639–642.  
1083 <https://doi.org/10.1130/G30883.1>
- 1084 Yunus, A. P., Fan, X., Tang, X., Jie, D., Xu, Q., & Huang, R. (2020). Decadal vegetation  
1085 succession from MODIS reveals the spatio-temporal evolution of post-seismic landsliding  
1086 after the 2008 Wenchuan earthquake. *Remote Sensing of Environment*, 236(October 2019),  
1087 111476. <https://doi.org/10.1016/j.rse.2019.111476>
- 1088 Zhang, F., Jin, Z., West, A. J., An, Z., Hilton, R. G., Wang, J., Li, G., Densmore, A. L., Yu, J.,  
1089 Qiang, X., Sun, Y., Li, L., Gou, L., Xu, Y., Xu, X., Liu, X., Pan, Y., & You, C.-F. (2019).  
1090 Monsoonal control on a delayed response of sedimentation to the 2008 Wenchuan  
1091 earthquake. *Science Advances*, 5(6). <https://doi.org/10.1126/sciadv.aav7110>

1092 Zhang, S., & Zhang, L. M. (2017). Impact of the 2008 Wenchuan earthquake in China on  
1093 subsequent long-term debris flow activities in the epicentral area. *Geomorphology*, 276, 86–  
1094 103. <https://doi.org/10.1016/j.geomorph.2016.10.009>

1095



*[Earth Surface]*

Supporting Information for

**[The Fate of Sediment After a Large Earthquake]**

[Oliver Francis<sup>1,2,\*</sup>, Xuanmei Fan<sup>3</sup>, Tristram Hales<sup>1,2</sup>, Daniel Hobley<sup>2</sup>, Qiang Xu<sup>3</sup>, Runqiu Huang<sup>3</sup>]

<sup>1</sup>Sustainable Places Research Institute, Cardiff University, Cardiff, United Kingdom

<sup>2</sup>School of Earth and Environmental Sciences, Cardiff University, Cardiff, United Kingdom

<sup>3</sup>State Key Laboratory for Geohazard Prevention and Geoenvironment Protection, Chengdu University of Technology, Chengdu, China

Corresponding author: Oliver Francis ([Oliver.Francis@gfz-potsdam.de](mailto:Oliver.Francis@gfz-potsdam.de))

\*Now at Section 4.7: Earth Surface Process Modelling, German Research Centre for Geosciences (GFZ), Potsdam, Germany]

**Contents of this file**

Figures S1 to S4  
Tables S1 & S3

**Introduction**

This file including the supporting information for The Fate of Sediment After a Large Earthquake. These support and provide further details of the methods and results described within the main text of the manuscript.

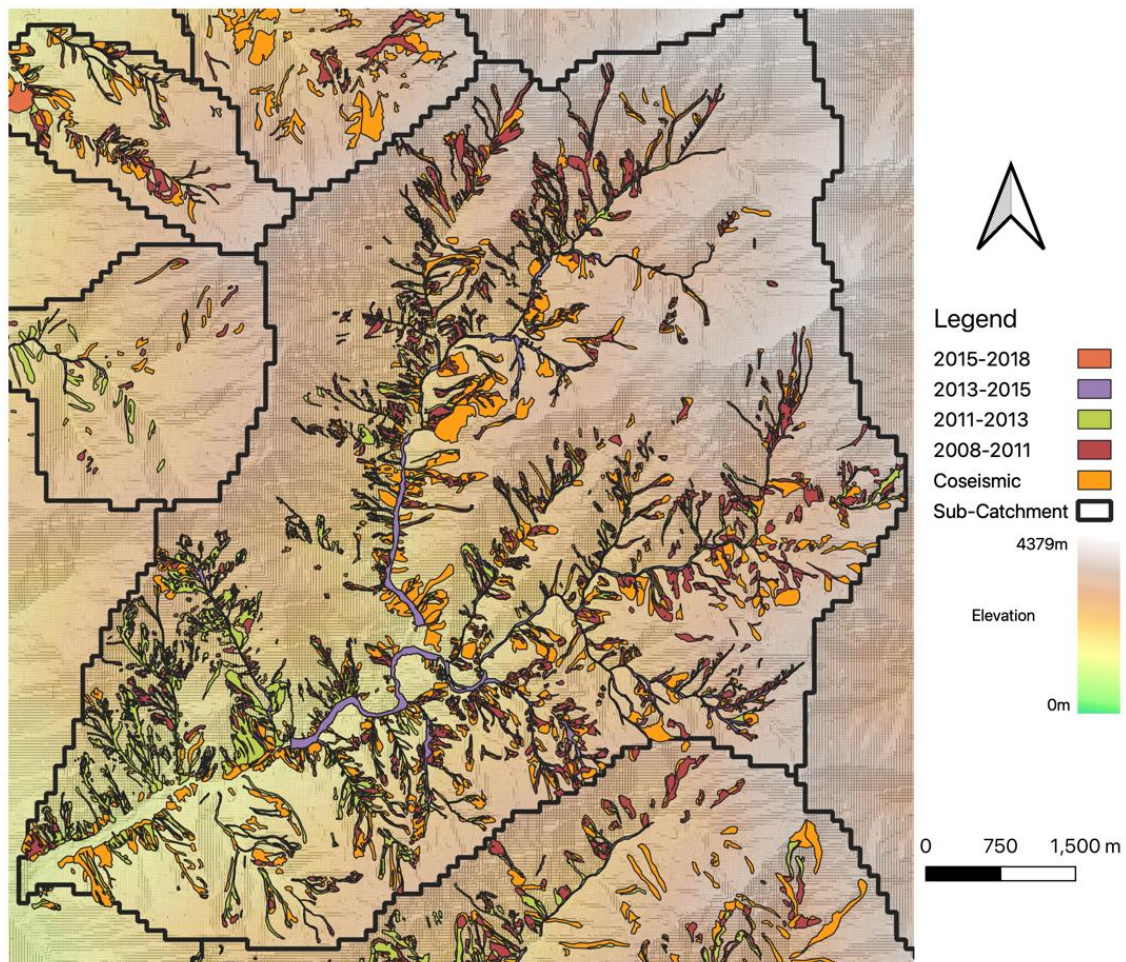


**Figure S1:** An example of a mapped catchment. Each mass movement is mapped as a polygon which is investigated for each epoch. The mass movement polygons are coloured based upon the epoch they were mapped in. Any mass movement which intersects with a mass movement from a previous epoch is defined as a remobilisation, if it does not intersect any previous mass movements it is defined as new.

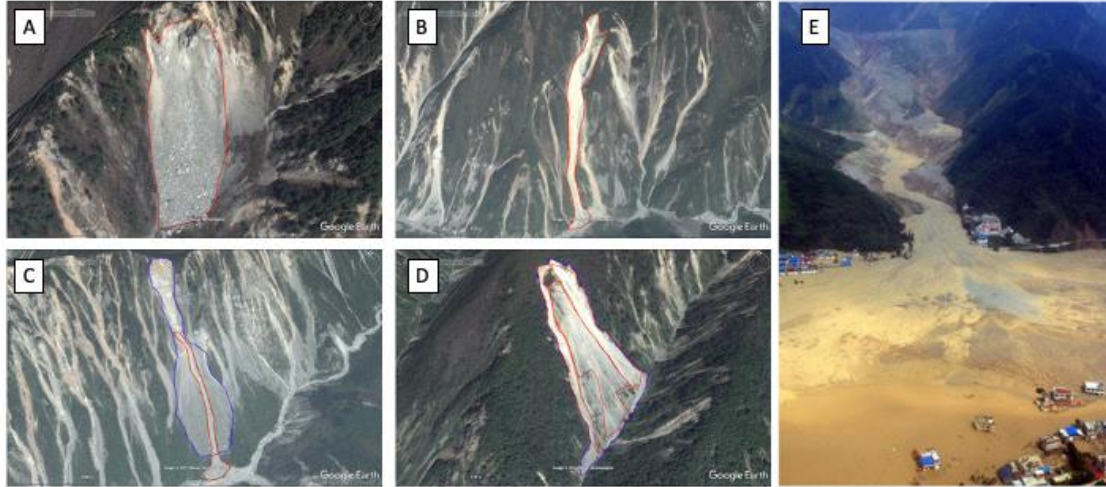


**Figure S2:** Examples of the main mass movement processes mapped within the mass movement inventory and an example of a catchment clearing debris flow. A) a mapped landslide, B) A mapped debris flow, C) a coseismic landslide which is then remobilised by a channelised remobilisation which deposits sediment into the tributary channels D) a coseismic landslide which is actively being remobilised but there no clear channelisation within the remobilisation. E) is a debris flow that occurred in 2010 which was triggered within coseismic landslide deposits in the Wenjia torrent and deposited over 1,000,000 m<sup>3</sup> of sediment directly into the Min Jiang. A,B,C,D are produced from Google Earth imagery while E is an aerial photo taken from (Tang et al., 2012).

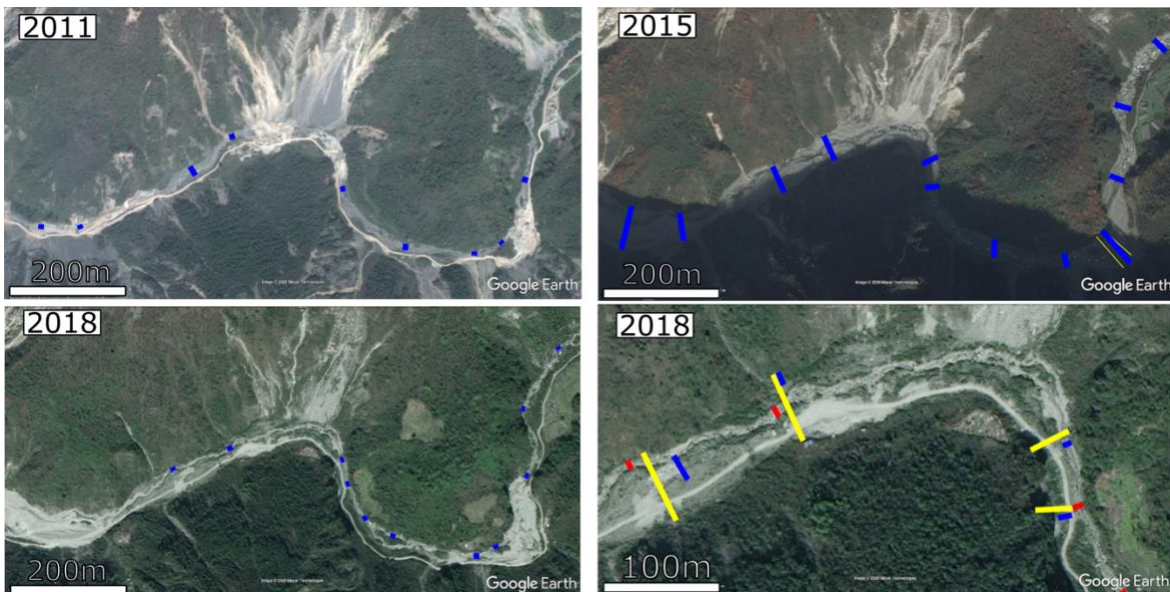


**Figure S3:** Examples of the mapping of tributary channel deposit cross sections. The first 3 images are of the same area through time. For each image the channel deposit is mapped to the edge of the visible sediment at regular intervals, shown in blue. The final image shows a subsection of a catchment with the mapped cross sections in different colours. The cross section from 2011 is mapped in blue, 2015 in yellow and 2018 in red. Due to rectification errors within Google Earth the cross sections are not in the exact same position, however care was taken to ensure repeat surveys were taken as close as possible.



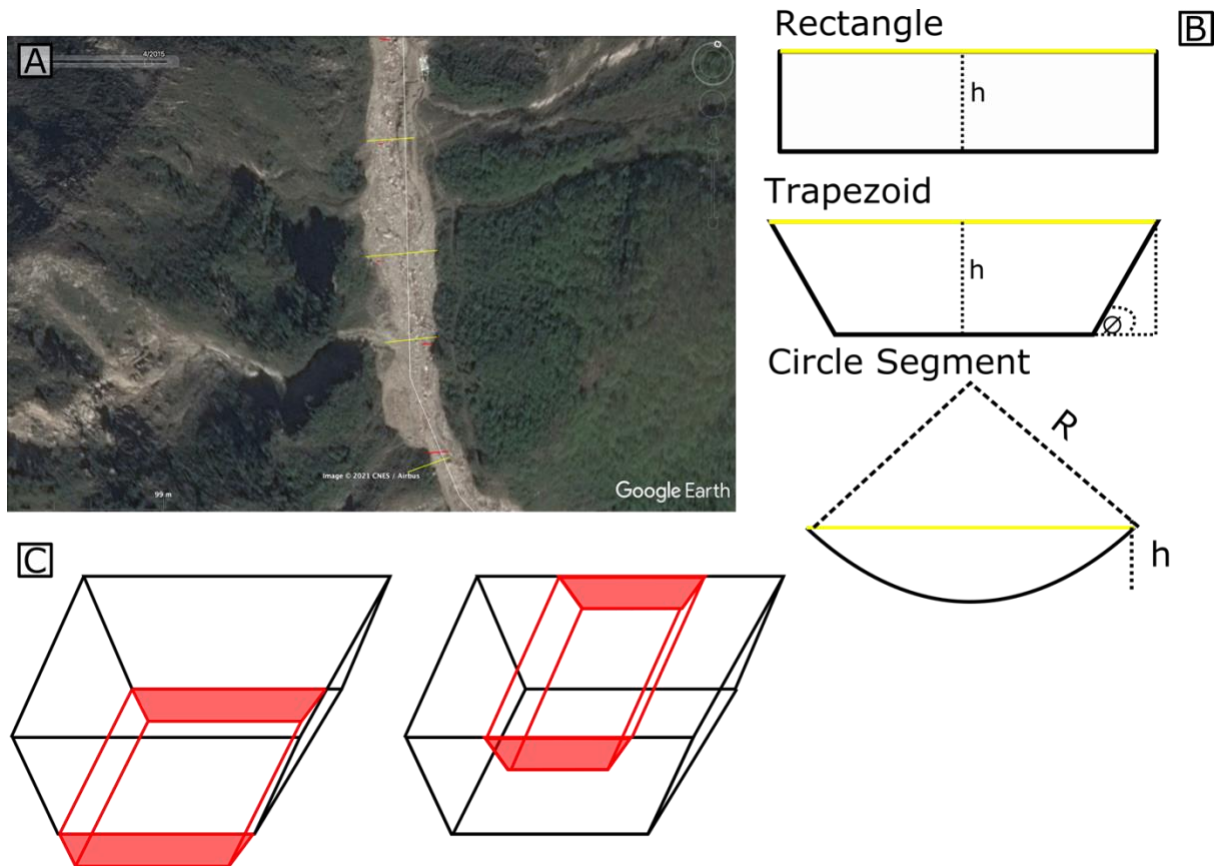


**Figure S4:** A demonstration of how the volumes of the channel deposits were estimated. A) a section of a surveyed tributary channel, the yellow lines indicate the width of the channel deposit in the year 2015 while red was mapped in 2011. Here each channel width has increased in size. The white line is used to estimate the distance between each channel width. B) The different shapes used for the cross-sectional area. The height of the rectangle and trapezoid was estimated by the width scaling ratio of (Moody & Troutman, 2002)  $h=0.27(w^2/7.2^2)^{0.39}$ . Simple trigonometry and angle relationships were used to determine the lengths of unknown sections. C) An example of how volume changes were estimated, if the width increases we estimate the volume deposited on top of the previous width (red), if the width remains the same we estimate the volume of sediment removed by the incision of the active channel which is reworking the sediment (shaded red). The volume is calculated by multiplying the added or removed cross sectional area by the distance between the measured widths.

Date of image	Source of Image	Resolution	Coverage
May – July 2008	Aerial photography	1 – 2.5m	97%

April 2011	Aerial photography and Worldview satellite	0.5 – 1m	99%
April 2013	Aerial photography and Pleiades satellite	0.5 - 2m	95%
April 2015	Spot 6 satellite	1.5m	99%
April 2017	Spot 6 satellite	3m	93%
April 2018	Spot 6 satellite	3m	93%

**Table S1.** The date, source and resolution of the images used in the development of the inventory. Coverage describes the percentage of the study area covered by the imagery at each time step.

Change in tributary channel deposits = New debris flows + Channelised remobilisation + Unchannelised remobilisation + Overland flow erosion – Incision – Suspended sediment – (0.5×Catchment clearing debris flows)	Equation 1
Debris flows (Channelised remobilisation + New debris flows) = Change in tributary channel deposits + Suspended sediment + Incision + (0.5×Catchment clearing debris flows) - Overland flow erosion – Unchannelised remobilisation	Equation 2

**Table S2.** The sediment budget of the tributary channel deposits and the equation used for determining the volume of the sediment mobilised by debris flows.

Frequency per year	2008	2011	2013	2015	2018
New hillslope deposits (debris flows)	462	24	20	4.5	0
New hillslope deposits (landslides)	8225	142	83.5	6.5	2.3
New tributary channel deposits	108	2.7	5	1	0
New Min Jiang deposits	35	0	0	0	0
Channelised remobilisation into the tributary channel deposits	0	112.3	67	16.5	1.6
Unchannelised remobilisation into the tributary channel deposits	0	200.7	92	10.5	3.6
Remobilised into the Min Jiang	0	4.3	4.5	0	0
Catchment clearing debris flows	23	37.3	5.5	0	0

**Table S3.** The average frequency of mapped mass movements for each mapped epoch. The number of catchment clearing debris flows is derived from (Fan et al., 2019)

References:

- Fan, X., Scaringi, G., Domènech, G., Yang, F., Guo, X., Dai, L., He, C., Xu, Q., & Huang, R. (2019). Two multi-temporal datasets that track the enhanced landsliding after the 2008 Wenchuan earthquake. *Earth System Science Data*, 11(1), 35–55.  
<https://doi.org/10.5194/essd-11-35-2019>
- Moody, J. A., & Troutman, B. M. (2002). Characterization of the spatial variability of channel morphology. *Earth Surface Processes and Landforms*, 27(12), 1251–1266.  
<https://doi.org/10.1002/esp.403>
- Tang, C., Van Asch, T. W. J., Chang, M., Chen, G. Q., Zhao, X. H., & Huang, X. C. (2012). Catastrophic debris flows on 13 August 2010 in the Qingping area, southwestern China: The combined effects of a strong earthquake and subsequent rainstorms. *Geomorphology*, 139–140(August 2010), 559–576.  
<https://doi.org/10.1016/j.geomorph.2011.12.021>